Lawrence Berkeley National Laboratory

Recent Work

Title

Berkeley Proton Linear Accelerator

Permalink

https://escholarship.org/uc/item/65r2z21p

Authors

Alvarez, Luis W.
Bradner, Hugh
Franck, Jack
et al.

Publication Date

1953-10-13

UNIVERSITY OF CALIFORNIA

Radiation Laboratory

BERKELEY, CALIFORNIA

DISCLAIMER

UNIVERSITY OF CALIFORNIA

Radiation Laboratory

Contract No. W-7405-eng-48

BERKELEY PROTON LINEAR ACCELERATOR

Luis W. Alvarez, Hugh Bradner, Jack Franck, Hayden Gordon,
J. Donald Gow, Lauristen C. Marshall, Frank F. Oppenheimer,
Wolfgang K. H. Panofsky, Chaim Richman and John R. Woodyard.

October 13, 1953

Berkeley, California

BERKELEY PROTON LINEAR ACCELERATOR[/]

Luis W. Alvarez, Hugh Bradner, Jack Franck, Hayden Gordon,
J. Donald Gow, Lauristen C. Marshall,[*] Frank F. Oppenheimer,[**]
Wolfgang K.H. Panofsky,[***] Chaim Richman and John R. Woodyard.

Department of Physics, Radiation Laboratory,
University of California, Berkeley, California

October 13, 1953

ABSTRACT

A linear accelerator, which increases the energy of protons from a 4 Mev

Van de Graaff injector, to a final energy of 31.5 Mev, has been constructed.

The accelerator consists of a cavity 40 feet long and 39 inches in diameter,

excited at resonance in a longitudinal electric mode with a radio-frequency

power of about 2.2×10^6 watts peak at 202.5 mc. Acceleration is made possible

by the introduction of 46 axial "drift tubes" into the cavity, which is designed

such that the particles traverse the distance between the centers of successive

tubes in one cycle of the r.f. power. The protons are longitudinally stable as

in the synchrotron, and are stabilized transversely by the action of converging

fields produced by focusing grids. The electrical cavity is constructed like

an inverted airplane fuselage and is supported in a vacuum tank. Power is

supplied by 9 high powered oscillators fed from a pulse generator of the

artificial transmission line type. Output currents are 3×10^{-9} ampere average,

and 50 µa peak. The beam has a diameter of 1 cm and an angular divergence of

10^{-3} radians.

---

[*]Now with the Link-Belt Co., Indianapolis, Indiana.

[**]Now at Pagosa Springs, Colorado.

[***]Now with the Department of Physics, Stanford University, Stanford, Calif.

BERKELEY PROTON LINEAR ACCELERATOR

Luis W. Alvarez, Hugh Bradner, Jack Franck, Hayden Gordon,
J. Donald Gow, Lauristen C. Marshall,[*] Frank F. Oppenheimer,[**]
Wolfgang K.H. Panofsky,[***] Chaim Richman and John R. Woodyard

Department of Physics, Radiation Laboratory,
University of California, Berkeley, California

October 13, 1953

I. INTRODUCTION

(1) Historical Summary. There was general agreement among physicists before the war that radio frequency linear accelerators of the Sloan-Lawrence[1] type were of historical interest only. This feeling arose largely because the cyclotron was found to be such a reliable device, with beam intensities far beyond the most optimistic hopes of its originators. At the same time, it was realized that to make a competitive linear acclerator for protons or deuterons would require far higher power than was then available at very short wavelengths. Although prewar r.f. linear accelerators are responsible for our present knowledge of the production of x-rays by high speed heavy ions, they played no part in increasing our knowledge of the nucleus. (Kinsey[2] reports that high speed Li ions impinging on hydrogenous material give the well-known alpha particles first observed by Cockcroft and Walton.)

Interest in linear accelerators was revived toward the end of the war for several reasons. Pressing military need had led to the development of vacuum tubes capable of producing megawatts of pulsed r.f. power down to the microwave range. The main technical bars to the construction of linear accelerators for electrons and light nuclei were thus removed.

But there would probably have been no great postwar interest in linear accelerators if the availability of the tools had been the only factor involved. It had been apparent for some time that there was an upper energy limit for particles accelerated by a cyclotron. The 184-inch cyclotron was originally

designed with the purpose of extending that limit as far as possible, but the goal was only about 100 Mev deuterons, even though a dee voltage in the neighborhood of 1.5×10^6 was to be used.

Since no significant theoretical limit is apparent for linear accelerators, it was felt that they should be reinvestigated as a means of reaching energies in excess of 100 Mev. Similar reasoning was applied to the electron case, where the betatron was known to have a practical energy limit only a few times greater than that of the cyclotron. No electron linear accelerators had been built before the war, but a description of the type now operating in a number of laboratories was given in 1941 by D. H. Sloan.[3] Such accelerators have been treated in detail by several authors,[4] and as they present quite different problems, they will not be discussed in this article on proton accelerators.

The situation as outlined above was drastically altered in 1945 by the introduction of the synchrotron concept.[5] In principle this removed the cyclotron upper limit, and raised it considerably in the betatron case to about 2,000 Mev. Clearly the linear accelerator must have had some other apparent advantage to have remained in the picture. Although recent studies have shown that the original arguments for undertaking the construction of a proton linear accelerator were not basic, the state of the art at that time did not allow them to be contradicted in a convincing manner.

The argument was essentially as follows: The cost of a relativistic magnetic accelerator varies roughly as the cube of the energy, so long as the basic design is merely scaled in its linear dimension, proportional to the energy. On the other hand, the cost of a linear accelerator varies directly as the first power of the energy. If these cost vs. energy curves are plotted on double logarithmic paper, they will clearly be straight lines with slopes three and one. There will always be an intersection of the two lines, and

for energies greater than the "cross-over" energy, the cost of a linear machine

will be less than that of the circular machine. Since the cost of either machine

is quite high in this region, it was felt that even though a linear accelerator

might be more complex than a synchro-cyclotron, the design decision might have

to be made on economic grounds.

The new consideration which has altered our thinking in this matter is

that beyond a certain energy, the magnetic machines can be changed in basic

design. Instead of accelerating with constant field and changing radius, the

two conditions are reversed. The important change is that a ring magnet can

then be used. This ring-shaped magnetic machine, which is really a proton

synchrotron, was proposed by Oliphant in 1944, before the work of Veksler and

McMillan, but it was generally felt for some time, in this country, that

although Oliphant's plan was most attractive in many ways, so many unsolved

and serious problems were involved in its practical realization that other

alternative methods of attaining high energy protons should be explored.

Within the past few years, critical examination of the whole question by two

groups in this country has shown that without question, all the problems are

solvable. Therefore, both the Radiation Laboratory and the Brookhaven National

Laboratory have built such machines for protons.

To see how this factor alters the economic conclusions originally reached,

it can be shown that not long after the "magnetic cost line" has crossed the

"linear cost line," the former drops to a much lower cost value for the same

energy, and then rises again with slope equal to three. The arguments of

dimensional analysis are still theoretically sound; there will still be a

crossover at higher energies. But long before this point is reached, the

cost of either machine is so high that both are excluded on economic grounds.

In the fall of 1945, we started the design of a "pilot model" proton

linear accelerator to explore the possibilities of the method. No plans

were made for extending the length of the machine beyond the original 40 feet,

but it was assumed that this question would be explored after successful

operation of the first section. If at that time it appeared wise to continue

on to higher energies, such a decision could then be made. In view of the

present status of the proton synchrotron at Berkeley, no extension of this

machine is planned here.   It should be pointed out that at the present

time, we know of no technical reason which makes this extension impossible or

even difficult. In fact, J. H. Williams at Minnesota is now building a proton

linear accelerator of the same type, which is 100 feet long, and will give

protons of 65 Mev.[*]

For the moment, then, we are concentrating on using the 40-foot accelerator

as a research tool. The machine has a number of advantages over the synchro-

cyclotron as a physics research tool. In particular, the characteristics of

the external beam of the linear accelerator are most attractive. Eighty-five

percent of the beam is concentrated within a circle of 3 mm diameter; the

angular divergence of the beam is approximately 10^{-3}, and the energy homogeneity

is about 3×10^{-3}. The average external beam is about 10^3 times that of the

184-inch cyclotron, and the average external beam current density is about

10^6 times as great.

(2) <u>General Design Characteristics.</u> The general design characteristics

pertaining to linear accelerators have recently been discussed in detail by

Slater.[6] In particular, Slater points out that the attainable voltage V of

a linear accelerator of length ℓ being fed at a peak power P is given by:

$$V = KP^{1/2} \; \ell^{1/2} \; \lambda^{-1/4} \tag{1}$$

where λ is the free-space wavelength. The constant K depends on the detailed

geometrical arrangement, and numerical values for the Berkeley accelerator will

be discussed later. A linear accelerator contains essentially different types

---

[*]The British Atomic Energy Establishment is actively engaged in the design
of a 600 Mev proton linear accelerator.

of equipment whose cost is proportional either to: (a) length, (b) peak power, (c) average power, (d) energy per pulse. All these factors affect the choice of wavelength, length of the machine, and duty cycle of operation. The pulse length of a resonant accelerator, τ, is given by:

$$\tau \propto Q \lambda \propto \lambda^{3/2}, \tag{2}$$

in order to permit full build-up of field; in terms of energy per pulse, U, Eq. (1) therefore becomes:

$$V = K U^{1/2} \mathcal{L}^{1/2} \lambda^{-1} \tag{3}$$

The wavelength dependence of power requirement for a given voltage and length is therefore small ($\lambda^{1/2}$), but the wavelength dependence of energy per pulse, on which the cost of the pulse equipment depends, is large (λ^2). From the latter point of view, it is particularly desirable to choose a small wavelength. However, there are several reasons for using long wavelengths, so one must make a compromise. As is shown in the next section on cavity modes, the difficulty of maintaining the proper field pattern in a standing wave accelerator increases as the square of the cavity length to wavelength ratio. (This ratio is called the electrical length of the cavity.) A second reason for using long wavelength comes from the necessity of a sufficiently large drift tube aperture. This reason dominated our thinking when foil focusing was to be used, but now that grid focusing is used, it is of lesser importance than the electrical length argument.

The present accelerator is designed with $\lambda = 150$ cm (200 megacycles). An important reason for the original choice of this wavelength was the availability of surplus radar equipment in this range. Although this radar equipment is no longer used to power the accelerator, it appears that the original choice of wavelength was very fortunate.

It might appear as if the balance between length and power would be made by matching the cost of the length proportional items and the power (or energy) proportional items. Actually in this and all other machines under design, as much power per unit length is applied as is feasible, compatible with electrical breakdown or available power sources. For a machine of the type discussed here, this limitation originally permited energy gains of only about two to three million electron volts per meter. At higher gradients, x-ray emission from the machine requires that extensive shielding be employed. (The x-ray yield increases as about the sixth power of the gradient.) Recent studies at the Radiation Laboratory have shown that surface layers of pump oil are responsible for most of the electron emission at energy gains of three Mev per meter. The use of mercury or ion pumps permits "energy gradients" of more than twice this value to be employed, with practical values of x-ray emission and sparking rate.

The choice of duty cycle is dictated by considerations of power consumption, cavity cooling, and tube power dissipation. Increase in repetition rate will not appreciably increase the cost of the pulse equipment; the pulse length is therefore chosen to give a duration of the pulse equal to several "build-up times"; the repetition rate is then chosen in accordance with available power.

The injection energy in the Berkeley accelerator was chosen as 4 Mev. The reason for this choice was twofold: (1) 4 Mev is a reasonable voltage to attain with an electrostatic generator and the construction of such a machine was desirable at this laboratory as a general research tool. (2) At the time of design, it was intended to accomplish focusing by means of thin beryllium foils.[7] Multiple scattering in these foils[8] made it necessary to choose a high injection energy. The 10 Mev linear accelerator which is to inject protons into the 6 Bev "Bevatron" is designed to accept 500 Kev protons from a Cockcroft-Walton generator.

It operates in a most satisfactory manner at an energy gradient of 0.5 Mev per foot, at a wavelength of 150 cm. (There is no apparent reason why the injection energy could not be of the order of 100 Kev.)

II. CAVITY DESIGN

(1) <u>Basic Geometry</u>. A linear accelerator for protons starting from low velocities (β = v/c = .092, 4 Mev) cannot be practically constructed on the basis of loaded wave guide geometry as is done for electrons.[4] Loading which would reduce the phase velocity to this low figure would lead to excessive r.f. power loss. For this reason, loading as such is not used. Instead, the phase velocity is made infinite, that is, the electric field is everywhere in the same phase, and small hollow conducting "drift tubes" are provided to shield the protons while the field is in the wrong direction. The drift tubes also cause a small amount of field perturbation which must be taken into account in designing the resonator.

The resonant cavity is essentially a long cylindrical cavity operated in the axial electric (0,1,0) mode, that is, the mode in which an axial electric field without azimuthal or transverse nodes is produced, as shown in Fig. 1. Efficient acceleration in a simple cavity is possible only if its axial length is shorter than $\beta\lambda/2$ where λ is the free-space wavelength corresponding to driving frequency, which, excepting for very low voltage machines, is not feasible. For this reason, the drift tubes previously mentioned are introduced coaxially in the cylinder, as illustrated in Fig. 2, with the distance between centerlines AB of successive drift tubes equal to $\beta\lambda$. If the gap g between drift tubes is short compared to $\beta\lambda/2$, the voltage gain of the particle can be nearly equal to the peak r.f. voltage developed across the gap. Note that the particle takes one full r.f. period to travel between midpoints of successive drift tubes. Each drift tube is charged oppositely at each end, (no net charge on

any tube) and all drift tubes are excited in phase. In the long wavelength Sloan-Lawrence accelerator[1] (Fig. 3), the drift tubes have alternately plus and minus net charges, and the distance between drift tube midpoints is $\beta\lambda/2$, rather than $\beta\lambda$ as it is in the cavity accelerator.

The general field geometry in the "unit cell" ABBA is very nearly the geometry of a doubly re-entrant symmetrical cavity excited in the lowest mode, such as is used in klystron resonators, T.R. boxes, etc. The entire accelerator can therefore be considered as being a juxtaposition of such cells repeatedly excited in such a phase that the current flowing on opposite sides of the joining faces AB (see Figs. 2 and 4) cancels. Such a picture would be exact if each successive cell were identical to the previous one; however, due to the progressive change in β corresponding to the gain in energy, the field distribution of the actual accelerator will not be exactly that corresponding to the distribution if the walls AB were actually present. For purposes of design, however, experimental and theoretical data based on single cell structure models are entirely adequate.

The joining of the unit cells is possible if each cell is accurately tuned to the same frequency. The tolerance of the tuning of the individual cell will be discussed later. Published design figures[9] on the resonant frequencies of this type of geometry are not of sufficient range to be used here, and also the details of the mechanical support structure of the drift tubes and similar deviations from ideal geometry made it necessary to derive the data pertaining to the resonant frequency of the unit cell from models. The resultant data[10] are shown in Fig. 5, using the notation as indicated in Figs. 2 and 4. The data are plotted in terms of dimensionless ratios to permit easy scaling. These data can be fitted by the empirical equation:

$$\frac{g}{L} = (-1.271) + (1.63)\frac{D}{\lambda} + (1.096)\frac{L}{\lambda} + (3.58)\frac{d}{\lambda} \qquad (4)$$

in the range of application used here.

It is clear that as the energy, and hence β and L/λ increases, the diameter d of the drift tube decreases; this decrease will eventually lead to a point where the design becomes impractical due to insufficient beam aperture and excessive curvature at the end of the drift tubes, with consequent high surface fields. For this reason, the diameter D of the outer cavity must be chosen small enough to conform to this limitation for the highest values of β; if chosen too small, the drift tubes on the low β end will become too large in diameter with consequent increase in losses. In the 40' linear accelerator described here, it was possible to compromise between these two extremes by the choice $D/\lambda = .66$. (Note that an unloaded cylindrical cavity is resonant at $D/\lambda = .766$.) If low energy injection had been used, it would probably have been impossible to find a satisfactory compromise on the diameter of the cavity which would have permitted the use of "reasonable" drift tube geometry at the two ends of the cavity. The cure for this would have been to use a tapered cavity, which would have increased the mechanical problems in fabricating the cavity. To build a multi-cavity accelerator for high energies, one would no doubt employ cavities with smaller diameters in the higher energy sections.

(2) <u>Voltage Gain and Input Power</u>. The voltage gain per unit cell is determined by three factors: a) geometry, b) power input, c) phase of particle transit.

Let N be the crest value of the magnetic flux circulating in the unit cell.* It can then be shown easily that the voltage gain in the unit cell is then given by:

$$V = \omega N \cos \phi \; \frac{\sin \frac{\pi g}{L}}{\frac{\pi g}{L}} \tag{5}**$$

if the electric field lines are assumed to be parallel across the gap; here

---

*Since the magnetic field is everywhere in phase in the mode used here, N can be defined uniquely as the surface integral of the crest value of the magnetic induction.

**MKS units are used throughout.

ϕ is the transit phase angle relative to the phase

of a particle crossing the center of the gap at the time of maximum voltage.

On the other hand, ωN is given in terms of the power losses in the walls

(and beam loading, here considered negligible) by a relation of the form:

$$N = \sqrt{2PZ_1} \tag{6}$$

where Z_1, the shunt-impedance/unit cell, is determined by the geometry and

the skin depth of the cavity wall material. For a continuing structure, Z_1

is proportional to the length; e.g., for a cylindrical, unloaded cavity of

length ℓ excited in the axial electric $(0,1,0)$ mode, the shunt impedance

is given by (neglecting end-losses):

$$Z_0 = \frac{.491\ell}{\delta} \sqrt{\frac{\mu_0}{K_0}} = 185 \frac{\ell}{\delta} = 185 \left(\frac{\ell}{\lambda}\right) Q_0 \text{ ohms} \tag{7}$$

where $a = \lambda/2.61$ is the radius, and $\delta = \sqrt{\frac{2}{\omega \mu_0 \sigma}}$ is the skin depth of the walls

of conductivity σ, and where $Q_0 = a/\delta$ is the conventional Q-value of the

cylindrical infinite cavity. To judge the merits of comparative drift tube

structures and to estimate the voltage gain as a function of power input, it

is therefore necessary to evaluate the shunt impedance per unit length (Z_1/ℓ)

of the loaded cavity relative to the similar quantity for the unloaded cylindri-

cal structure as given above. This evaluation was done semi-empirically by

mapping the magnetic field B across the azimuthal plane of the cavity, by

means of an exploring loop, as shown in Fig. 6. The shunt impedance Z_1 and

the Q are then obtained by numerical evaluation of the integrals:

$$Z_1 = \sqrt{\frac{\mu_0}{K_0}} \frac{4\pi}{\lambda \delta} \frac{\left(\int_{\text{Cross section of field}} B dA\right)^2}{\int_{\text{Surface}} B^2 dA}$$

$$Q = \frac{4\pi}{\delta} \frac{\int_{\text{Field}} B^2 r \, dA}{\int_{\text{Surface}} B^2 \, dA} \tag{9}$$

Typical resultant values* of Q and Z_1, tabulated relatively to the unloaded

cavity values, are given below. (Table I.)

Proton Energy (Mev)	$\beta = L/\lambda$	Z_1/ℓ ohms/meter	Z_0/ℓ ohms/meter	Q	Q_0
50	.315	41×10^6	3.75×10^6	106,000	117,000

Frequency 148 m.c.

Table I

The resultant values of Z_1, Z_0, Q and Q_0 require an additional correction factor

of approximately $1/(1+ a/\ell)$ to correct for end losses in the cavity. Note that

the shunt impedance/unit length of the loaded cavity as calculated from the field

plots is actually slightly larger than that of the unloaded cavity, and the Q is

slightly less, although the difference is probably within the accuracy of the

measurements. (The simple theory of the variations of Q and Z indicates that

they should go in the observed direction.)

The loss values arrived at by the flux plotting method are obviously lower

limits, since losses in the drift tube support structure, pumping slots, joints,

etc., are not taken into account. However, a simple measurements of the experi-

mental Q of the cavity will give a measurement of the true shunt impedance also,

since Z and Q are reduced in the same ratio. The resultant values, arrived

at by experimental measurement of Q are given in Table II, computed for the

entire accelerator.

	Q	Z(ohms)	Power for $V = 28$ Mev**(watts)
From flux plot	106,000	457×10^6	1.40×10^6
From Q measurement	72,000	311×10^6	2.06×10^6

Table II

---

*Experimental values are probably accurate to ± 10 percent.

**Taking $\phi_s = 30°$, $g/L = .25$ (see Eq. (5)).

(3) <u>Modes of a Long Cavity</u>. In designing the accelerator cavity from data obtained on unit cells, a definite assumption has to be made pertaining to the voltage gain per cell. In order to join the cells without partition, the wall currents, and therefore the wall magnetic fields, must be continuous. Since, as shown by magnetic flux plots, the ratio of total flux per unit length (and therefore voltage gain per unit length) to the magnetic field at the edge varies by only 20 percent from the injection end to the output end of the accelerator, (the ratio being higher at the high voltage end) it was decided to design the accelerator for constant voltage gain per unit length, which results in a 20 percent "taper" of magnetic field along the cavity walls. The constancy of the voltage gain per unit length is of course also desirable in order to equalize the surface gradient along the accelerator and to reduce the tendency to spark.

In order to assure equality of the mean electric field in a coupled structure involving 47 individual resonators, the individual resonators must have very accurately the same resonant frequency. This can only partially be assured by the model "unit cell" measurements referred to above, since: (a) the extension from unit cells to the long accelerator of varying units is not exact, and (b) slight mechanical changes from the model geometry will interfere with exact transfer of the data, and (c) the accuracy (approximately .05 percent) of the model frequency measurements is not quite sufficient. For this reason it is necessary to adjust the final field distribution to its value required for acceleration by correction applied to the cavity as a whole.

The behavior of the cavity can best be described by means of its mode spectrum. The operating modes of the machine is on the lower edge of the pass band of the cavity used as wave guide, and therefore the mode separation varies quadratically as the limit is approached. Specifically, for an unloaded cavity,

the spectrum is given by:

$$f_n = f_0 \sqrt{1 + \left(\frac{nc}{2f_0 L}\right)^2} \tag{10}$$

where f_0 is the frequency of the lowest mode. The low end of the spectrum of
the 40-foot accelerator cavity is plotted in Fig. 7. Owing to the small mode
separation (.17 percent) near the limit, two problems have to be considered:
a) the possibility of "mode jumping" to an adjacent mode, and b) the tolerances
in geometry required to assure that the lowest mode has the desired field pattern.
These appear at first sight to be independent, but it will be shown shortly
that they are different aspects of the same problem. The first is solvable
by proper disposition of the exciting oscillators or by careful tuning, and will
be discussed later. The second can be analyzed by a simple perturbation calculation
in which we assume that the actual field distribution excited in a single mode
can be expanded in terms of the modes of a cavity whose mode distribution is
the desired one,* hereafter called the "ideal" cavity.

A detailed derivation of the perturbation theory equations would be out of
place in this report.[11] Instead, an outline of the method of attack will be given
together with the final working equation. The long cavity is treated as a hollow
structure of circular cross section; the radius varies as a function of z, and
is given by the Fourier series:

$$a_z = a_0 \left\{ 1 + \sum_{i=1}^{\infty} P_i \cos \frac{i\pi z}{L} \right\} \tag{11}$$

In the case of an actual linear accelerator cavity, the natural frequencies of
the various unit cells will vary as a function of z. The connection between the
theories of the two types of cavities comes from the fact that in the hollow
cavity, the natural frequency of a given section is related to the radius by
the equation:

$$f_z = \frac{0.383c}{a_z} \tag{12}$$

---

*Such an expansion is always possible since the normal modes in a cavity form
a complete orthogonal set of functions.

We express the axial electric field in the hollow cavity as:

$$E_z = J_o(k_z r) \, e^{j \omega t} \, E_o \left\{ 1 + \sum_{n=1}^{\infty} \epsilon_n \cos \frac{n \pi z}{L} \right\} \tag{13}$$

This field must satisfy the following differential equation:

$$\frac{1}{r} \frac{\partial}{\partial r} \left\{ r \frac{\partial E}{\partial r} \right\} + \frac{\partial^2 E}{\partial z^2} + \frac{\omega^2 E}{c^2} \left(1 + \frac{j}{Q} \right) = 0 \tag{14}$$

The boundary conditions are introduced through the requirement that $J_o(K_z a_z) = 0$, (tangential electric field = 0 at a conductor). This requirement introduces Eq. (11) into the problem.

The solution of the problem shows that the coefficient ϵ_n depends only on the coefficient $P_i = P_n$; a cavity with only an nth harmonic radius variation will have only an nth harmonic perturbation in the field pattern of its operating field. The magnitude of ϵ_n is related to that of P_n by the equation:

$$\epsilon_n = \frac{8N^2}{n^2} P_n , \tag{15}$$

where N is the "electrical length" of the cavity, L/λ. To show the relation between field distortion and mode separation in an ideal cavity, Eq. (15) may be combined with Eq. (10), to yield:

$$\epsilon_n = \frac{f_o}{f_n - f_o} P_n \tag{16}$$

(All of these equations are approximations which are good for low modes in long cavities.)

N is 8.3 for the present accelerator, so:

$$\epsilon_n = \frac{550 \ P_n}{n^2} \tag{17}$$

It is apparent from Eq. (17) that a first harmonic tuning error of a given amplitude, $-P_1$,* will give rise to a first harmonic field error 550 times greater.

---

*It should be noted that P_n was defined as the Fourier coefficient of the radius variation; by Eq. (12), it will have opposite sign when used as the tuning error coefficient.

The "amplification factor," $8N^2/n^2$, is of such a form that tuning errors in the high harmonics do not distort the field patterns appreciably. As an example of the high degree of accuracy with which the various cells in the accelerator must be tuned, we will calculate the permissible first harmonic tuning error, if the field is to be "flat" to $\pm$ 5 percent (ϵ_1 = 0.05). P_n = 0.009 percent. This means that the average frequencies of the two halves of the accelerator must be the same to within about one part in 10^4. (The corresponding tolerance on drift tube lengths is about 0.001"!) This is too severe a tolerance to be met mechanically, even if the design data were accurately enough known. In practice, the "end tuners," or variable length half-drift tubes at the two ends of the cavity, are used to alter P_1 and P_2. Such alterations can be made while the cavity is excited at its operating field strength, by motor controls. These adjustments need be made only after the accelerator has been opened for adjustments; they are stable for weeks during operation.

The last paragraph was concerned with the problem of keeping the accelerator in adjustment. The more serious problem is in first putting it into such a condition that Eq. (15) may be used as a guide for the final adjustments. If the two halves of the cavity were de-tuned from each other by one percent, the value of ϵ_1 would be greater than unity. Since the equations were developed from a perturbation theory ($\epsilon_n << 1$) they are no longer applicable when $P_1 \approx 1$ percent. Since such errors were present in the newly constructed accelerator cavity, they had first to be eliminated by another procedure. A moveable "end wall" was placed between two centrally located drift tubes. The resonant frequencies of the two halves of the cavity were then measured independently. The positions of the drift tubes were altered by small amounts so that the two halves of the cavity had the same natural frequency. The same procedure was repeated with quarter length segments of the accelerator.

After these preliminary adjustments, the cavity could be excited to give a
perturbed "zeroth mode" field pattern (Fig. 8a). This field pattern was Fourier
analyzed, and the coefficients ϵ_n were determined. From Eq. (16), the tuning
error coefficients, P_n, were determined. Using these coefficients, a Fourier
synthesis yielded the tuning error as a function of z (Fig. 8c). Model work
yielded $df/d\ell$, the variation in natural frequency of a given unit cell with
drift tube length. The tuning error curve together with $df/d\ell$ gave a "drift
tube length error curve." Mechanical shims were constructed according to this
last curve, and inserted under the removable ends of the individual drift tubes.
The new field pattern, which was acceptably flat, is shown in Fig. 8b.

The discussion above has been simplified to the extent of treating the
axial electric field as proportional to the surface magnetic field. This is
very nearly so, but the constant of proportionality changes slowly along the
length of the accelerator. It is a simple matter to "tilt the field pattern"
under operating conditions, by the use of the end tuners, so one can ignore
the small lack of constancy of $\left[E_z/H_{\phi}\right](z)$. In practice, one tilts the field to
yield a proton beam at the lowest threshold electric field in the cavity.

If the accelerator cavity were to be made 3.15 times longer than it is,
N^2 would be 10 times as great. This would cut the frequency separation of the
lowest two modes to one-tenth of its present value (340 KC/10 = 34 KC). The
modes would still be distinct, since the width of the tuning curve is of order
$f/Q = 2 \times 10^5$ KC/8 $\times 10^4 \approx 3$ KC. Mode jumping would therefore not be a problem,
even though the modes were 10 times closer. However, a cavity 10 times as
long as the present one would have problems connected with mode jumping. (One
could not assure that the field pattern would be constant in time, since the
tuning curves of the lowest modes would overlap.)

The effect of increase length on the field pattern in the operating mode
also goes as N^2, or inversely as the mode separation. If the cavity were $\sqrt{10}$
times its present length, the tolerances could probably be met by attention to

detail, but if the cavity were 10 times as long, the problem of maintaining a

flat mode would probably be too severe. The last paragraph shows that mode

jumping difficulties would come in at about the same length. It might be

thought that these problems could be circumvented by making several independent

cavities, which were tightly coupled. However, the same problems exist in that

case. If accelerators of this type are to be built with large values of N,

they will probably have several independent cavities fed by a master oscillator

and power amplifiers, rather than by the self-excited oscillator used with

our accelerator. The independent cavities could easily be kept tuned to the

master oscillator by a servo system, and then individual short lengths would

make the field flatness problem easy of solution. The Minnesota accelerator

is designed according to these ideas.

(4) <u>Experimental Field Plots</u>. A three dimensional picture of the complete

field plot as obtained by the magnetic loop method is shown in Fig. 9. Note

that the resultant fields are a mixture of fields of the coaxial type ($1/r$

dependence near the drift tubes) and the TM_{01} type $\left[J_1(kr) \right]$ dependence in the

gaps.

For use in transit time and focusing calculations, the electric field $E(Z)$

along the axis is needed. As will be explained later, the entrance of each

drift tube is closed with a focusing grid while the exit end is open. For this

reason, theoretical analysis of the field is difficult and an experimental procedure

is used. This procedure consists in measuring the frequency shift produced by

placing a small metallic object of volume δV at various points in the field.

The disturbed frequency is given by:[12]

$$f^2 = f_0^2 \left\{ 1 + A \int_V (H^2 - E^2) \, dv \right\} \qquad (18)^*$$

where A is a constant depending on the geometry of the metallic object.

---

*W. W. Hanson and R. F. Post, Journ. App. Phys. <u>19</u>, 1059 (1948).

H^2 and E^2 are normalized to unity over the total volume of the cavity.
If the measurement is made along the axis, $H = 0$ and:

$$\frac{f^2 - f_o^2}{f_o^2} = -\frac{\int_{\delta V} E^2 dV}{\int_{cavity} E^2 dV} \tag{19}$$

$$\frac{\triangle f}{f} = K\, E^2\, \delta V \tag{20}$$

An axial field plot for a typical drift tube geometry is shown in Fig. 10.
These data were taken on a 1000 mc scale model using a heterodyne frequency
measuring method. The metallic sphere was supported on a stretched thread.

III. BEAM DYNAMICS*

(1) General Equations of Motion. A particle of charge e and mass M_o, traveling
in the linear accelerator, is acted on by both radial and longitudinal forces.
The longitudinal forces are due to the axial component of the radio frequency
electric field; the transverse forces are due to a) the transverse radio frequency
electric field and b) the effect of the radio frequency magnetic field.

In order to know the motion precisely, the electric field components $E_z(r,z,t)$,
$E_r(r,z,t)$ and the r.f. magnetic field $B_\phi(r,z,t)$ have to be known. For a sinusoidal
time variation the equations of motion are:

$$\frac{d}{dt}\left[\frac{M_o}{\sqrt{1-\beta^2}}\frac{dz}{dt}\right] = e\left[E_z^o(r,z,t)\cos(\omega t+\phi) +B_\phi^o(r,z)\frac{dr}{dt}\sin(\omega t+\phi)\right] \tag{21}$$

$$\frac{d}{dt}\left[\frac{M_o}{\sqrt{1-\beta^2}}\frac{dr}{dt}\right] = e\left[E_r^o(r,z)\cos(\omega t+\phi) -B_\phi^o(r,z)\frac{dz}{dt}\sin(\omega t+\phi)\right] \tag{22}$$

The superscript ^{o} denotes the amplitude of the respective fields. If exact
results are needed one has to integrate these equations numerically using empirical

*For details of the calculations presented in this section see UCRL-1095.

fields. However, many general facts about the nature of the motion can be learned without exact integration.

In general, as Eqs. (21) and (22) show, the radial and longitudinal motion of a particle on the linear accelerator are coupled. This coupling is important if the energy gain per gap depends markedly on the radial position, which would be the case if one has relatively large drift tube apertures; also in the early stages of the accelerator where the phase motion, (z motion) has not yet damped out, there is considerable coupling between the radial and axial motions. However, if the drift tube apertures are small, which is the case of interest, one can find some reasonable approximations to the phase motion by integrating the equation at constant r. Since the resulting phase motion damps rapidly with N it is also possible to arrive at a useful solution for the radial motion.

(2) Synchronous Conditions. The basic geometry of the linear accelerator is shown in Fig. 11. At a given time the electric fields are everywhere in phase and the magnetic field is in quadrature with the electric field. Let L_n be the "repeat length" of the nth gap and g_n be the gap length. In crossing the nth gap the velocity of the particle changes from $C\beta_{n-1}$ to $C\beta_n$ (Fig. 11). The coordinate z is measured from the "electrical center" of each gap; this center is defined by the condition:

$$\int_L E_z(z) \sin\left(\frac{2\pi z}{L}\right) dz = 0 \tag{23}$$

For a symmetrical gap, this definition corresponds to the geometrical center. The phase of a particle ϕ_n is the number of radians in time by which the particle crosses the electrical center of the nth gap relative to the time at which the electric field is at its maximum value. Let

$$\Phi_n > 0 \tag{24}$$

correspond to a particle crossing after the maximum field has been reached and

$$\Phi_n < 0 \tag{25}$$

to a particle crossing before. These definitions agree with Eqs. (21) and (22).

In order to simplify the discussion we will assume that the machine is constructed so that for certain injection conditions the phase ϕ_n of the particle at each gap is independent of n. This particle is called a synchronous particle and all quantities associated with this particle, energy, momentum, etc., will be denoted by a subscript s. The phase angle ϕ_s is called the synchronous phase. In principle, the machine cannot be designed to have a synchronous particle without knowing the motion; the motion cannot be determined without knowing the fields in the machine. In particular, if fractional velocity change per gap is large, the design can only be done by successive approximation. However, if the fractional velocity change is small then the synchronous condition will be:

$$\frac{L_n}{\lambda} = (\beta_{n-1,s} + \beta_{n,s})/2 \tag{26}$$

λ = free space wave length.

The synchronous particle will increase its total relativistic energy by:

$$W_{n,s} - W_{n-1,s} = \int e\, E_z^0 \cos\left(\frac{\omega z}{V_s} + \phi_s\right) dz \tag{27}$$

V_s is the synchronous velocity. In general, using the definition of the electrical center, we can write Eq. (27) as:

$$W_{n,s} - W_{n-1,s} = e\,\lambda\, T\, E_o \left(\frac{\beta_{n,s} + \beta_{n-1,s}}{2}\right) \cos \phi_s$$
$$= e\, T\, E_o\, L_n \cos \phi_s \tag{28}$$

where

$$E_o = \int_{gap} E_z^0(z)dz \Big/ \int_{gap} dz \tag{29}$$

is the mean effective field, and:

$$T = \int E_z^0(z) \cos\left(\frac{2\pi z}{L_n}\right) dz \Big/ \int E_z^0(z)dz \tag{30}$$

is the "transit time factor." For a "square wave" field which is uniform in the gap and zero in the drift tubes:

$$T = \sin\left(\frac{\pi g_n}{L_n}\right) \Big/ \frac{\pi g_n}{L_n} \tag{31}$$

If one also considers the radial variation of T, one finds that for the square wave field and a drift tube bore of $2A_n$ one has:

$$T = \frac{I_0\left(\frac{2\pi r}{L_n}\right)}{I_0\left(\frac{2\pi A_n}{L_n}\right)} \; \frac{\sin\frac{\pi g_n}{L_n}}{\frac{\pi g_n}{L_n}} \qquad (32)$$

The additional factor is due to field penetration into the drift tubes, and is a factor producing coupling between the radial and axial motions.

A basic design parameter of the machine is the energy gain per wave length in $M_0 c^2$ units:

$$W_\lambda = \frac{e \, E_0 \, T\lambda}{M_0 c^2} \cos \phi_s \qquad (33)$$

In terms of the parameter, Eq. (28) in the non-relativistic range can be written as:

$$\beta_{n,s} - \beta_{n-1,s} = W_\lambda \qquad (34)(\text{N.R.})$$

In the relativistic range the fractional changes in velocity will be small and therefore if we write $W_{n+1,s} - W_{n,s} = \Delta W_{n,s}$ it follows that the momentum increment $\Delta P_{n,s} = V_{n,s} \Delta W_{n,s}$ and therefore it follows that relativistically:

$$P_{n,s} - P_{n-1,s} = M_0 c \, W_\lambda \qquad (34)$$

which includes (34)(N.R.). From Eq. (34) it follows that <u>the momentum is a linear function of the number of drift tubes.</u> Hence, we can write for the synchronous particle:

$$P_{n,s} / M_0 c = (n+n_0) W_\lambda \qquad (35)$$

$$W_{n,s} / M_0 c^2 = \sqrt{1 + (n+n_0)^2 \, W_\lambda^2} \qquad (36)$$

Here n is taken to make n = 1 the first gap of the machine and n_0 is the "effective number of gaps" corresponding to the injector.

(3) <u>General Stability Considerations for a "Long" Accelerator.</u>

    a. Types of Stability.

      To obtain satisfactory operation for a "long" linear accelerator it is clearly necessary that the orbits be stable in phase and also stable radially.

What length of such an accelerator would be considered "long" in this sense
depends of course on the tolerances on injection conditions, voltage gradient, etc.,
which can be held. We shall show later that the periods of the various oscillations
depend on the number $N = n+n_o$, i.e., the total effective number of drift tubes
including the injector. A linear accelerator of this type is thus "long" in the
sense of requiring stability if it increases the injection momentum by a large
factor. A large injection voltage thus tends to make an accelerator effectively
"short."

Phase stability is produced in a linear accelerator if a late particle receives
a large degree of acceleration. This, in the case of a linear accelerator, means
that the particle would traverse the center of each gap at a time when the field
is increasing.* Specifically, the condition for phase stability in a field
$E_z(z, \omega t)$ is:

$$\frac{\partial}{\partial \phi} \left\{ \int E_z \left(z, \frac{\omega z}{V} + \phi \right) dz \right\} > 0 \qquad (37)$$

The conditions for radial stability are more complicated. Focusing is obtained
by the following mechanisms: 1) velocity focusing, sometimes called electrostatic
or second order focusing, 2) phase focusing, 3) focusing produced by charges
or currents contained within the beam.

   b. Incompatibility of simultaneous radial and phase stability.

If no charge is contained in the beam, a particle crossing a gap will cross
as many lines directed towards the axis as away from the axis. A net radial
momentum is thus produced if: a) the particle changes its velocity when crossing
the gap, and b) if the field varies in time. The former mechanism is the one
which accounts for the focusing in electrostatic lenses. In the accelerator this
effect is important only in the first few gaps of a machine with low injection
energy. The second effect rapidly becomes dominant in the later gaps. It is
clear that the condition for phase focusing is that the field be decreasing

---

*Note that this is the inverse of the condition pertaining to phase stability
 of a circular accelerator.

during the passage of the particle across the gap. This condition appears

incompatible with the phase stability condition expressed by Eq. (37). McMillan[13]

has shown that this disagreement is a fundamental one, and cannot be removed by

artifice in geometry.

    c. Radial oscillations.

The incompatibility between radial and phase stability can be removed if:

1) the velocity of the particle changes appreciably in crossing the gap. 2) the

entrance to the next drift tube is closed by a grid or foil. (Fig. 12.)[*]

It can be shown that the change in velocity can account for a small region

of phase stability without grids or foils. However, the analysis shows that

even if the particle crosses the center of the gap at the crest of the r.f.

wave, the time of passing the entrance and exit of the gap are not symmetrical

with respect to the time of passing the center; the particle spending more time

approaching the center than leaving the center. Due to the time variation of

the field the focusing field at the entrance will be weaker than the defocusing

field at the exit. This effect increases with the gap length and counteracts

the effects of velocity focusing. In fact there is a critical gap length

beyond which velocity focusing becomes negative (defocusing).

The second method of achieving radial and phase stability, by use of grids

and foils, is more important in actual accelerators. The field configuration

of Fig. 12 will obviously give a net inward momentum change to a particle

accelerated across the gap.

It can be shown that this momentum change is given by:

$$\Delta P_r = - \frac{er}{2V^2} \left\{ VE_F - (1-\beta^2)\, \omega \frac{\partial}{\partial \phi} \int E_z\left(z, \frac{\omega z}{V} + \phi\right)\, dz \right\} \quad (38)$$

E_F is the electric field at the foil at the time of passage of the particle through

the foil. This term can only be evaluated for a particular field. Calculations

for the "square wave" field show that foil or grid focusing give rise to stable

---

[*]To these conditions can be added: 1) external focusing devices, such as strong
  focusing lenses[14] and the use of a periodic modulation of the synchronous phase
  angle[15,16]. The latter, when analyzed in detail[15] requires a very precise control
  of radio frequency field amplitude.

radial oscillation in the phase region:

$$-\frac{\pi}{2}\left(1 - \frac{2g_n}{L_n}\right) < \phi < \pi/2\left(1 + \frac{2g_n}{L_n}\right)$$

Fig. 13 shows the region of stable focusing and phase stability for $g_n/L_n = .25$; the motion is completely stable for $-\frac{\pi}{4} < \phi < 0$. If $\frac{g_n}{L_n} > \frac{1}{2}$ foil or grid focusing is ineffective. An asymptotic solution for the radial oscillation can be obtained for large n.

$$r_n \propto \beta_n^{1/4} \; e^{\pm i \int^n \frac{K^{1/2}(\phi)\, dn}{(n+n_0)^{1/2}\left[1 + (n+n_0)^2 \; W_\lambda^2\right]^{1/4}}} \tag{39}$$

$$K = \frac{\pi}{2 \sin \frac{\pi g_n}{L_n}} \; \frac{\cos\left(\frac{\pi g_n}{L_n} - \phi_n\right) - 2\beta_s^2 \sin \frac{\pi g_n}{L_n} \sin \phi_n}{\cos \phi_n} \tag{40}$$

Non-relativistically one can obtain exactly:

$$r_n = \sqrt{N} \left\{A \; J_1\left(2\sqrt{K_s N}\right) + B \; Y_1\left(2\sqrt{K_s N}\right)\right\} \tag{41}$$

This has been plotted for $n_0 = 24$ and various values of ϕ_s in Fig. 14.

The effects of small angle multiple scattering in the case of foil focusing have been treated by Serber.[8] The limit on the transparency of the grids which can be used is set by the field concentration on the grid wires.

d. Phase oscillations.

The nature of the phase oscillations has been investigated analytically and the following expressions have been obtained which describe the phase motion in the non-relativistic and extremely relativistic ranges:

$$\phi_n \propto \frac{1}{N^{(3-2G)/4}} \cos\left(2\sqrt{-2\pi \tan \phi_s}\; \sqrt{N} + \delta\right) \tag{42}(N.R.)$$

where $G = 1 - \frac{\pi g_n}{L_n} \cot \frac{\pi g_n}{L_n}$.

$$\phi_n \propto \frac{1}{N^{3/4}} \cos\left[2\left(\sqrt{-2\pi \tan \phi_s}\;/W_\lambda\right) N^{-1/2} + \delta\right] \tag{42}(E.R.)$$

where $\phi_n = \phi_n - \phi_s$.

Thus in the extreme relativistic region the phase motion becomes non-oscillatory as demanded by the asymptotic constancy of velocity.

Whether or not a particle, injected into the machine, will be accelerated

through the machine depends on the phase and velocity which it has at the entrance

to the machine. Calculations of the phase acceptance of a linear accelerator are

summarized in Fig. 15. This is a plot of ϕ_n vs. $n_o^{1/2} \Delta W/W_o$, the characteristic

parameter for this phenomenon, for various ϕ_s. $\frac{\Delta W}{W}$ is the fractional variation

in injection energy. Any particle inside one of the closed curves will be phase

stable but not necessarily radially stable. It can be seen that for lower injection

energies (smaller n_o) the tolerances on the injection voltage becomes less critical.

e. Unstable operation.

It is clear that if a linear accelerator is short enough it can be operated

without grids. It will then be either phase unstable or radially unstable. The

original r.f. linear accelerator of Sloan and Lawrence was clearly operated in

such a manner. Experiments with the 40-foot linear accelerator without grids

have shown that one can obtain an "unstable" beam of essentially the same magnitude

as is obtainable with grids. However, the criticality of adjustment is greatly

increased.

IV. MECHANICAL DESIGN

(1) Tank. The resonant cavity of the accelerator is housed in a vacuum

tank 40 feet 6-1/2 $\pm$ 1/4 inches long and 48-1/2 $\pm$ 1/4 inches diameter (inside

dimensions), made of welded 1/2 inch boiler plate, with flat steel ends 1-1/4

inches thick. The tank is divided longitudinally 4 inches above center, and

the top lid is hinged at four points along the north side to permit the lid

to be opened for access. Provisions for vacuum seal of the lid are described

in Section IV(3) of this report. Opening of the lid is accomplished by a pair

of hydraulic cylinders mounted near the middle of the lid, and anchored to the

pump manifold, which is a protuberance from the bottom half of the tank, on

the north side. The entire tank is supported on two pads, each 1/4 of the way

from an end of the tank. The east end pad rests on a 2-foot long 2-inch diameter

steel bar which can roll east-west on a steel plate that in turn is fastened

to the concrete floor. The west end pad rests on two similar bars which give

some rotational stability to the tank. The 2-foot long bars are sufficient to

keep the tank from falling over, but additional stability against rotation is

provided by resting the pump manifold on the floor. The tank is thus mounted

so that it can expand freely with temperature changes.

The resonant cavity is also mounted so that it is free to expand and

contract with temperature changes independently of the steel tank. In the

southeast and southwest corners of the tank, groove pads with the groove pointed

east-west are mounted at the height of the middle of the liner. In the north

center of the tank there is a similar pad with its groove oriented north-south.

The liner is not sufficiently rigid to be supported at just these three points,

so 15 spring loaded pads with hardened flat ground surfaces are equally spaced

around the sides of the tank to distribute the support points. On the liner,

there are 3/8 inch bolts with hardened steel balls soldered to the ends so that

the resonant cavity is supported at 18 points, of which three constrain its

position and motion. This elaborate mounting was installed after it was noticed

that the steel vacuum tank warped in places as much as 1/2 inch when the lid

was raised and lowered. Methods of accommodating for this warp in the attachments

between liner and tank, i.e., r.f. transmission lines, water cooling lines, and

end tuning motors, are indicated elsewhere in this report.

The tank, opened by the hydraulic lifts, is shown in Fig. 16.

(2) Liner Design. With the decision to separate the mechanical and

electrical functions of the linear accelerator resonant cavity, came the need

for the design of an accurate, rigid, and light weight tubular lining for the

vacuum tank. This "liner" became a structure basically similar to a monocoque

airplane fuselage of frame, stringer, and sheet construction save that the sheet

surfaces were on the inside. Since it was desired to avoid circumferential

joints in the sheet surfaces, and since the cross section was constant, it

became practicable to roll copper strip stock into pannels of the length of

the liner, with flanges and corrugations to serve as longitudinal stringers.

By using die-formed circumferential frames with a polygonal inside cross section,

the longitudinal panels could be flat and the necessary dimensional tolerances

could be more easily maintained. The cross section of the liner as situated

in the tank is diagrammed in Fig. 17. The liner is of dodecagon cross section

of 38-1/8 inch dimension across flats, 480 inch length and split longitudinally

into two unequal parts, of 150° and 210°, to permit support of the lower part

along the horizontal centerlines.

(3) <u>Liner Construction.</u> The longitudinal copper panels were rolled from

an .032 inch thick by 13 inch wide by 60 foot long copper strip to have a flange

turned up at each edge and to have a semicircular channel in the center to

receive a 5/8 inch copper cooling-water tube. A total of 40 "pump out" slots

one-half inch wide by 12 inches long were used, with the slots strapped every

four inches. Thirty-three circumferential frames were made in two parts from

.072 inch 24 ST aluminum alloy. The internal flange, to which the copper

attached, was made of short lengths of extruded angle riveted to the frame.

Clearance cutouts for the cooling tubes and drift tube supports were provided

and reinforced where necessary by attached angles. The frames were finished

with an aircraft zinc and chromate primer.

Support rails for the drift tubes were run from end to end of the liner

through cutouts in the frames. These rails were interrupted every 30 inches

to allow for differential thermal expansion. Openings for the drift tube stems

could then be cut through the copper panel at any point without interference

with frame position. Support of the drift tube was accomplished by two clamp

plates that were placed on each side of the salient flange of the angles that

formed the rail. (Fig. 18.) Three-inch diameter holes were punched in the end

and the side of the liner, opposite glass viewing ports in the vacuum tank.

This allows one to observe sparking and other related phenomena in the liner.

Vertical aluminum braces are attached between the end of the liner and the "end tuner" structure, to provide rigidity to the tuner. An end tuner consists of a drift tube extending into the resonant cavity from the end of the liner, with length controllable by a worm gear which is driven by a flexible shaft leading to a motor outside the vacuum tank. Electrical contact is made between this drift tube and the end of the liner by means of a tight fitting slotted collar of silver-plated steel, fitting around the drift tube, and bolted to the liner. The west end (entrance) tuner drift tube is 4.750 inches diameter, and adjustable in length from 2 inches to 4 inches. The east end tuner drift tube is 2.750 inches diameter and 4 inches to 7 inches long.

(4) <u>Drift Tube Construction and Support.</u> The drift tubes are basically a cylinder of variant length and diameter, supported by a single stem perpendicular to the liner axis at the center line of each drift tube. The drift tube diameter varied from 4-3/4 inches to 2-3/4 inches, the first eleven drift tubes being constant at 4-3/4", and the remaining 35 drift tubes diminishing to 2-3/4", in steps of approximately sixty-thousands of an inch. The drift tube lengths vary from about 4-3/8" for the first drift tube to 11 inches for the last drift tube. The drift tube body is made of a copper tube, with the end at the beam exit made from a copper plate hard soldered into the tube, and with a threaded ring in the opposite end. Into this threaded ring is screwed a cap, which in turn receives a grid holder. The exit end of the drift tube has a re-entrant opening, formed by a brass tail tube about 3 inches in length, and varying from 1 inch inside diameter to 1-1/2 inches inside diameter, for the range of drift tube sizes. All external edges are uniformly rounded with a radius of 3/8 inch. The threaded cap was originally designed to be screwed into the drift tube body after the grid holder had been inserted from the inside. On the initial runs, serious sparking was found to have occurred across the contact surface between the drift tube cap and body, even though special effort had been taken to

insure high contact pressures at this point. Thus it became necessary to solder

the drift tube cap to the body with a low temperature eutectic alloy, and to

redesign the grid holder so that it could be inserted from the front of the drift

tube. The threaded construction, however, did permit the drift tube lengths

to be changed by shims after the voltage distribution measurements were completed.

The drift tube stems are made of one inch diameter brass tubing, soft soldered

into a reamed boss on the transverse center line of the drift tube. Through this

stem is passed a quarter inch diameter copper tube, that makes a loop around the

inside of the drift tube body to which it is soft soldered, and then returns

through the stem for circulation of cooling water. The use of brass stems was

found to be a mistake, and it was subsequently found necessary to silver plate

the drift tube body and stem, to reduce r.f. losses in the brass stem and tail tube.

The drift tube stem is closed by a plug which carries a threaded extension. The

drift tube components are diagrammed in Fig. 19.

The drift tubes are supported (see Fig. 18) by a pair of plates which clamp

on the salient flanges of the drift tube support rails supported by the liner

frames. One of these clamp plates has a large clearance hole, while the other

is provided with a seat for a spherical washer, and with four tapped holes uniformly

spaced about the seat. The threaded extension of the drift tube stem passes

through a cross of steel, heat treated to a spring temper, and then through a

hemispherical washer, where it is terminated with a nut. With the hemispherical

washer resting in the seat provided in the clamp plate, and with four cap screws

through the threaded holes bearing against the arms of the cross, the drift tube

is held firmly in position, and can be adjusted along the three coordinate axes

by means of the two pairs of screws on opposite sides of the stem, and by means

of the two pairs of screws on opposite sides of the stem, and by means of the

nut on the threaded extension.

(5) <u>Liner and Drift Tube Cooling.</u> A semi-circular distribution manifold is soldered to the end plates of the liner on both top and bottom parts. From this manifold radial tubes lead to fittings on the ends of the 40 foot tubes soldered to each liner panel; thus, the panels are cooled by water flowing through these long tubes in parallel, in circuits that come through the tank at one end, through the distribution manifold, along the panels into the collection manifold, and out through a discharge lead at the opposite end of the tank. Separate circuits are maintained for the upper and lower parts of the liner.

The drift tubes are also cooled in parallel by a third water cooling circuit. Two tubes are supported in openings in the liner frames, with one tube serving as supply header, and the other as collection header. These tubes have nipples hard soldered to them adjacent to each drift tube, into which the 1/4 inch copper tube passing through the drift tube stems are soldered. By introducing the water at one end of the tank and removing it from the other, the cooling water pressure drop through each parallel flow path is maintained the same. Checks upon the operation of the parallel flow system are made by putting hot water through the lines, and feeling all the tubes to see that they are receiving their quota of water, and that no obstructions exist in the individual circuits.

(6) <u>Grids.</u> As was shown in Section III of this paper, radial focusing and phase stability can only be achieved in the machine by introducing charge within the beam; i.e., by arranging the entrance end of drift tubes so that electric field lines terminate within the beam. This was first done by putting 3×10^{-5} inch thick beryllium foils across the entrance of each drift tube. However, sparking in the tank destroyed them, and grids were used instead. There is, of course, greater field concentration on grids than on flat foils. To a first approximation, if one considers a grid to be merely a foil with many holes punched out, the field is increased by a factor equal to the ratio of the total area to the area occupied by conductors, since the same number of lines of force end on the conductor, but on a smaller area.

The ratio of aperture to field strength can be improved by using a slat
grid of structure similar to a klystron grid, instead of a perforated plate, since
some of the field line will terminate on the flat sides of the slats. Fig. 20
shows several grid shapes which have been used, and also the beryllium foils.

Grids were fabricated from .002 x 1/16 inch tungsten ribbon. A 95° bend was
put in short sections of this strip by means of modified vise-grip pliers. Copper
rings mounted on a carbon mandrel were slit by a multiband saw to a depth of 72
mils. The bent strips were put into these slots and hard soldered around the
rim, which was then given a finishing lathe cut. The grids were polished to
approximate the optimum "rounded" shape, by immersing in 2 molar NaOH and
passing 5 amps. a.c. for 5 seconds between the finished grid and a tungsten rod.
They were next soldered with pure tin copper holders which hid the brass ring,
and could be screwed into the entrance end of the drift tubes. Grids were given
a thorough visual inspection through a 30x stereoscopic microscope, and sharp
points were removed. Then they were tested by photometering the transmission of
a beam of parallel light from a tungsten strip filament lamp. The optical path
was: pin hole over strip filament lmap, collimating lens, grid, focusing lens,
.010 inch diameter pinhole, photronic cell. It is interesting to note that this
was a "good geometry" experiment, so that an aperture of, say, 90 percent of
the total opening gave a photocell reading of 80 percent.*

The final test of the grids was made by investigating their behavior in
vacuum under d.c. field equal to the r.f. field of the linear accelerator. If
the cold emission was less than 50 μa after the grids had been given up to
5 minutes run-in time, they were accepted. A grid in its mounting is shown in
Fig. 21. At the present time, the grid aperture has been considerably increased
by removing all but the four central L shaped slats. No significant increase
in the x-ray background from the tank accompanied this change, which shows that
field emission from other parts of the drift tube is still responsible for most
of the electron drain in the machine.

* i.e., the diffracted component of the beam is not recorded by the photocell.

In practice, we do not believe that the etching procedure was necessary. We tested several grids electrically, which had not been etched, and could not find any significant difference from the normal ones.

The 15 cycle r.f. pulses produce fields of 10^7 volts/meter between the drift tubes, or 4 gm/cm^2 on the drift tube ends. This pulsed force is sufficient to loosen the grid holders, so set screws are used to lock them into the drift tubes.

(7) Radiation Shielding. The stray radiation around the linear accelerator has been investigated to determine its sources and energies. The radiation comes almost entirely from x-rays produced by electron bombardment of the drift tube ends. These sources were determined by exposing x-ray plates through an iron slat collimator "telescope" laid on top of the accelerator. The energies of the x-rays near the exit end of the accelerator were found by absorption measurements to be up to 2 Mev, corresponding to electrons passing through one or two gaps between No. 45 drift tube and the end of the liner.

One-half inch of lead shielding hung on frames near the sides and top of the linear accelerator has reduced the x-ray level, measured two feet from the machine, to ⌣10 MR/hr. The shielding has many openings, such as holes for the transmission lines, and a four-foot wide space below the Pb, so that there is scattered radiation throughout the room. The level 30 feet from the machine is ⌣5 MR/hr.

Three inches of lead glass are provided over the tank windows through which the inside of the liner can be viewed.

After the tank has been let down to air and re-evacuated, the radiation level is higher by a factor of 2 to 5, but improves quickly with running of the r.f. which serves to outgas the system. Outgassing can also be speeded by running hot water through the liner cooling lines, though that has very seldom been done. After the accelerator has been run for several months,

the x-ray level has slowly risen by a factor of five, due to oil deposits on the drift tube surfaces. (Fig. 22.) The tank is usually opened about twice a year to clean off the oil deposits.

(8) Vacuum System. The basic requirements of the linear accelerator vacuum system are, first, a base pressure 10^{-5} mm or less, and second, a pump-down and bake-in time of reasonable length, say, 8 hours. To fulfill these conditions in a steel tank 40 feet long, of 15,000 liters capacity, containing about 500 vacuum seals and joints, and several hundred feet of polyethylene cable, it was obviously necessary to provide a fast pump, and keep leaks and outgassing to a minimum. That this has been done successfully can be seen from the fact that at present, the base pressure is about 2×10^{-6} mm, the rate of pressure rise with the pumps closed off is as low as 10^{-7} mm/sec., and bake-in times as short as 4 hours have been recorded.

Pumps. The pumps used are a 30 inch three-stage diffusion pump with a pumping speed of 7000 liters/sec and an 8 inch two-stage diffusion pump in series, backed by two 43 c.f.m. Kinney rotary mechanical pumps in parallel. The diffusion pumps use Litton oil, which is effectively kept out of the tank by a thorough refrigerated baffling system. The pumping speed measured inside the liner is 2,500 liters/sec, which is considered a reasonable fraction of the speed of the pump alone.

Seals and Joints. A very wide variety of seals is used on the linear accelerator. Besides the usual types, such as soft and hard solder joints, gaskets, and arc-welded seams, there are Wilson seals, sylphon seals, aircraft-type spark plugs, and even certain standard r.f. connectors which have been found to be vacuum-tight.

Perhaps the most noteworthy of the gasket seals is the main tank gasket, which runs completely around the tank and is almost 90 feet long. To eliminate the expense of machining a flange 40 feet long it was decided to use a molded rubber gasket held to the flange with special screws and retained by a 1/4 inch

square strip of steel tack-welded to the flange along the vacuum side (Fig. 23).

Despite the un-machined flange, the performance of this gasket has exceeded

our expectation. Three bolts on each side suffice to hold the flanges together

and when the pumps are started, the external air pressure exerts ample force

to complete the seal. The heads of the screws act to separate the flanges and

prevent them from damaging the gasket.

Vacuum Seals and Joints. The vacuum seal to the outside of the radio

frequency transmission line is made with a standard 4" diameter rubber "O-

ring," (see Fig. 25). This seal and the transmission line are installed and

removed totally from the outside of the vacuum tank. This seal seldom leaks,

although there is some motion of the transmission line in it due to the

differential thermal expansion between the liner and the vacuum tank and the

warping of the tank due to the change in pressure during pump down.

The vacuum seal to the inner conductor of the transmission line is made

with flat teflon gaskets in compression between the insulator and the copper

conductors that make up the transmission line.

V. OSCILLATORS

The present machine was designed to operate with an average voltage

gradient of .90 megavolts per foot, or a total end to end voltage of 36 mega-

volts (peak value). This differs from the energy gain (28 Mev) of the particles

due to the operating phase angle and transit time loss. Since the shunt

impedance of the liner on the fundamental mode is 316 megohms, the radio

frequency power required by the accelerator is approximately 2.1 megawatts.

Since the machine is pulsed "on" for 600 microseconds, fifteen times per

second, i.e., a duty cycle of 111, the average power is approximately 20

kilowatts.

The accelerator was first put into operation in October, 1948, using eighteen and later twenty-six power oscillators, each of which developed approximately 85 kw from four GL-434 triode tubes in parallel connection.

The GL-434 tubes, which were obtained on war surplus, had such a high casualty rate while in operation, with many actually becoming gassy on the shelf, that it was decided to build an oscillator system using a more rugged tube.

The oscillator system now in use was installed in February, 1950, and consists of three pre-exciter oscillators and nine single tube power oscillators each connected to the liner through a separate transmission line and coupling loop.

The present pre-exciters consist of some slightly modified radar type "BC-677" oscillators which are loosely coupled to the liner. These exciters perform three important functions for the machine: They excite the liner through the multipactor region, they select the correct mode of oscillation and they supply the low level of radio frequency energy to the liner necessary to start the power oscillators.

The multipactor action is almost universally found in devices using high radio frequency voltages in a vacuum. This is a secondary electron multiplication process which can produce severe loading at low power levels, but once the system is above that level it disappears. To illustrate this process, consider two parallel metal plates spaced some small distance apart in a vacuum. In general the secondary electron emission ratio for metals (with the usual surface contamination) will be greater than unity. If an increasing radio frequency voltage is applied between the plates, there will be found one value of voltage such that an electron can just cross the gap in exactly one-half cycle. If the energy of the electron is of the correct magnitude more than one secondary electron will be released and these electrons will see a voltage

such as to accelerate them back across the gap again where they will make still more electrons. This process builds up very rapidly and can dissipate a large amount of energy. With the geometry found in the accelerator the multipactoring limits the voltage to very low amplitudes.

The straightforward cures are to make the electron transit time different in the two directions by a d.c. bias, or to raise the radio frequency voltage so rapidly that there are not enough r.f. cycles in the critical region for the discharge to become large. The low energy end of the machine provides extremely favorable geometry for such a discharge between drift tubes. The spacings between the drift tubes in this region are of the order of an inch and it can be shown that this gap will be resonant for multipactor action at around 2000 volts. In addition there are many such gaps, any one of which can be responsible for the discharge.

The first cure attempted was to isolate every other drift tube from ground for d.c. and to apply a bias such as to make the transit time different in one direction from that in the other. This method worked, but brought with it many difficulties in providing a suitable radio frequency by-pass condenser from the drift tube stems to the liner.

About this time the problem was solved by the experimental discovery that three pre-exciters coupled in at the high energy end of the liner (where the drift tube spacings are the longest and the most unsuitable for multipactoring) could deliver sufficient energy (taking advantage of the very low group velocity of propagation in the liner as a waveguide at cutoff) to drive the rest of the liner up through the multipactor voltage region so rapidly that the multipactoring did not have time to build up.

The correct mode is selected by careful manual tuning of the three loosely-coupled pre-exciter oscillators.

The main oscillators will not start without the low level pre-excitation because the energy storage or "fly-wheel effect" of the liner is large and their power gain for small signals is low.

The pre-exciters establish the correct mode at low level (approximately 1% of final power) by being pulsed on 30 to 100 microseconds before the main oscillators are turned on. This operation cycle is indicated in Fig. 24.

Each of the nine power oscillators uses an Eimac tube type 3W10000A3 in a modified "Colpitts" circuit. The oscillator is made of coaxial transmission lines. The inner (drive circuit) and the outer (plate circuit) coaxial lines connect the tube to the load (coupling loop in the liner) through the output transmission line. The relative characteristic impedances and the lengths of these lines control the amplitudes and phases of the radio frequency voltages appearing on the tube and load circuits. The physical layout is shown in Fig. 25, and Fig. 26 is the schematic equivalent oscillator circuit diagram.

The magnitude of the load impedance is adjusted by varying the size of the coupling loop in the liner. The self-inductance of this coupling loop is purposely designed to be so small that the coupled impedance of the liner at resonance dominates. These loops are copper plates 6" long, 6" wide and spaced approximately 3/8" from the wall of the liner. The impedance of the self inductance of these loops at 200 mcs is approximately 15 ohms and the coupled impedance from the liner is approximately 150 ohms. The importance of this impedance ratio is qualitatively illustrated in Fig. 27. The coupling loop presents only the impedance of its low self inductance to the oscillator for frequencies which are near but not on the liner frequency. This low impedance, upsets the magnitudes and phases of the voltages within the oscillator and discourages it from oscillating. In addition, the magnitudes and phases of the voltages appearing at the tube vary so rapidly with frequency that oscillation is discouraged for frequencies somewhat removed from the liner frequency.

Each oscillator unit rests on, and is partially enclosed by, a metal cabinet with interlocked doors for personnel protection. (See Figures 28 a, b.) All high voltage, air cooling and water cooling connections are made inside this cabinet and are designed to be quickly disconnected. The "quick disconnect" idea was also applied in designing the "plug in" connection between the oscillator and the coaxial transmission that feeds the radio frequency power from the oscillator to the liner.

This "quick disconnect" feature allows a faulty oscillator to be replaced in approximately five minutes.

Each oscillator is pre-tested at a peak power output of more than 350 kw (duty cycle of 111, plate voltage 18.5 kv, overall efficiency of 50%) although in actual operation it delivers 250 kw (plate voltage 15 kv).

The present oscillator system had 4400 hours of "beam on" time in the 22 months to November, 1952, compared to 2100 hours in the 30 months that the original system was in use.

VI. THE POWER SYSTEM

(1) General Description. Available electrical components, cooling require-ments and general power requirements dictate that the accelerator be operated as a pulsed machine. The pulse length (600 μ sec maximum) is a compromise between cavity build-up time and available energy storage capacity. As high a duty as is permissible by power considerations is desirable from the point of view of minimizing accidental coincidences in coincidence counting experiments.

For the parameters involved here, energy storage in rotating machinery is not practical. Accordingly, the system adopted is a pulse forming synthetic transmission line continuously charged through a reactor.

The approximate design specifications of the power supply are given in Table I.

	MAIN SUPPLY			
	per oscillator		total	
	peak	average	peak	average
D.C. input power	450 kw	3.9 kw	4000 kw	3.5 kw
voltage	14.0 kv	14.0 kv (peak)	14.0 kv	14.0 kv (peak)
current	32 a	.28 a	290 a	2.5 a
R.F. output power	250 kw	2.2 kw	2200 kw	20 kw
Impedance	$R_{dc} = \dfrac{V_p}{I_p} = 440 \ \Omega$		$R_{dc} = \dfrac{V_p}{I_p} = 49 \ \Omega$	
Cathode Power	3.4 kw		30.6 kw	
Repetition Rate	15 cps			
Pulse length	600 μ secs			

	PRE-EXCITER SUPPLY			
	per oscillator		total	
	peak	average	peak	average
D.C. input power	180 kw	1.1 kw	530 kw	3.5 kw
voltage	10 kv	10 kv (peak)	10 kv	10 kv (peak)
current	18 a	.11 a	53 a	.35 a
R.F. output power	7 kw	.05 kw	21 kw	.15 kw
Impedance	$R_{dc} = \dfrac{V_p}{I_p} = 560 \ \Omega$		$R_{dc} = \dfrac{V_p}{I_p} = 190 \ \Omega$	
Cathode Power	1.2 kw		3.6 kw	
Repetition Rate	15 cps			
Pulse length	440 μ secs			

TABLE I

To fulfill these specifications it was decided to use combinations of a standard three-phase mercury vapor rectifier circuit charging a pulse forming network through a reactor. The network is discharged into the load by a triggered spark gap through a pulse transformer.

The power oscillators used in the present design require that the cavity be pre-excited before they can generate r.f. power. This requires a separate power system to feed the pre-exciter oscillators; this system is identical in design to the "main" supply outlined above with the exception that the pulse forming network is charged through an emission limited diode in place of the reactor, and that no pulse transformer is used. The block diagram of the equipment is shown in Fig. 29.

(2) Pulse Forming Networks. The use of pulse forming networks became common usage in the later phases of radar practice and their design principles are well understood. As used here it is simply a synthetic open circuited transmission line composed of a finite number of sections. Fig. 30 shows the numerical constants employed here.

If such a line is charged to a voltage $2V_o$ it will store an energy of $2NV_o^2C$ where N is the number of sections of capacity C and inductance L. If the line is discharged into a load of its characteristic impedance $Z_o = \sqrt{L/C}$ the load voltage will be V_o and will last for a time $T = 2N\sqrt{LC}$. The total energy dissipated is thus equal to $TV_o^2/Z_o = 2NV_o^2C$ in agreement with the above. The output voltages, reflections under mismatch conditions can be studied by conventional transmission line theory.

The line shown in Fig. 30 differs from a simple line of identical sections by the design of its leading section. If the line were condenser terminated (π-section) the voltage on discharge would rise to $2V_o$ resulting in a bad voltage overshoot. If the line were inductance terminated (T-section) the voltage would

rise from zero and then overshoot. This difficulty is analogous to the overshoot phenomenon (Gibbs phenomenon) encountered in Fourier synthesizing discontinuous waveforms by a finite number of terms. The first section design, as suggested by William W. Hansen, is shown in Fig. 30. It assures that the impedance, as seen by the load on switching, shall be Z_0; overshoot is thus avoided.

(3) _Line-charging._ The electrical length of the pulse forming line is short with respect to the repetition interval; for purposes of charging, the line can thus be treated as a lumped capacitor.

If a capacitor is charged from a fixed voltage source through any non-reactive network, an energy equal to the stored energy is dissipated in the charging network. Hence if, in order to produce a constant rectifier current, the condenser bank is charged through an emission limited diode, half the supply power will be dissipated on the diode anode. This is the system used in the pre-exciter supply where power economy is not essential.

If a capacitor of capacity C is charged through a rectifier of voltage E in series with an essentially loss-less reactor, the capacitor will always be charged to a voltage V = 2E. This is required by energy conservation since the work done by the rectifier is C E V while the energy stored in the condenser is $CV^2/2$. If the reactor is loss-less this requires V = 2E. The mechanism of the doubling action will differ depending whether the half period

$$\mathcal{T} = \pi\sqrt{LC} = \pi/\omega_0$$

of the charging system is greater or less than the interval σ between pulses. The waveform occurring in the three cases $\mathcal{T} \gtrless \sigma$ are shown in Fig. 31. If $\mathcal{T} < \sigma$ (Case I) the charging cycle is a half period of the L-C circuit; the voltage is then clamped at a value 2E. If $\mathcal{T} = \sigma$ (Case II) the half cycles are just joined. If $\mathcal{T} > \sigma$ (Case III) which is the case used in the linear accelerator, less than a half cycle elapses between pulses. Since the charging current is essentially unchanged during the discharge period, the charging voltage and current waveforms

will be the portion of the appropriate sinusoid, symmetrical about the midpoint

of the charging interval. As $J \to \infty$ the charging cycle approaches a saw-tooth

wave. The principal advantage of a large value of J is the smaller current

fluctuation reflected in the power line. The principal hazard of a large J is

the large magnetic energy storage in the reactor. This results in a voltage

overshoot on the line in case the spark-gap accidentally does not fire. Voltage

overload protection is thus needed.

Table II presents the relevant design information of interest in charging

system design.

Case	$\dfrac{\text{Peak current}}{\text{Average current}}$	$\dfrac{\text{Reactor power loss}}{(\text{Av. current})^2 \times \text{Reactor resistence}}$	Voltage overshoot ratio
$J < \sigma$	$\sigma\pi/2J$	$\sigma\pi^2/8$	1
$J = \sigma$	$\pi/2$	$\pi^2/8$	1
$J > \sigma$	$(\pi\sigma/2J)\sin^{-1}(\pi\sigma/2J)$	$\dfrac{\pi^2\sigma^2}{8J^2}\sin^{-2}\left(\dfrac{\pi\sigma}{2J}\right)\left[1 + \dfrac{T}{\pi\sigma}\sin\left(\dfrac{\pi\sigma}{J}\right)\right]$	$\dfrac{1+\sin(\pi\sigma/2J)}{2\sin(\pi\sigma/2J)}$

TABLE II

(4) Spark Gaps and Pulse Transformer. The current switching is done by a

set of spark gaps. These gaps operate in air and are made of simple spherical

copper electrodes. An air jet de-ionizes the arc mechanically. The gaps are

mounted in a sound-proof box.

The main oscillators are matched to the pulse forming lines by a fast pulse

transformer. The transformer operates at a turn ratio of 2:1. It weighs approxi-

mately 2000 pounds.

The spark gaps are triggered by a 100 kv pulse of approximately .1 μ sec

duration. This pulse is provided by discharging a condenser through the primary

of a pulse transformer of the design of Kerns and Baker[17] by means of a hydrogen

thyratron. The grids of the thyratrons are driven by a central pulse generator.

This circuit delivers pulses to the pre-exciter and main oscillator thyratrons with the proper timing. The repetition rate can be set to any desired frequency, up to the limit imposed by the allowable duty cycle. The pulse generator supplies a trigger pulse to the Van de Graaff which keys the ion source on after the cavity is built up, and also supplies miscellaneous trigger pulses to actuate scope sweeps, counter gates, etc.

VII. ACCESSORY EQUIPMENT.

(1) <u>Electron Catcher Magnet and Monochromatizing Magnet.</u> The high axial r.f. electric fields existing in the resonant cavity can accelerate any free electrons, formed between drift tubes, to considerable energies, corresponding to approximately 60 percent of the voltage across the gap. Electrons formed near the exit end of the No. 46 drift tube by secondary electron multiplication or gas ionization can be accelerated to an energy of 1.1 Mev. These electrons constitute an appreciable personnel hazard and also interfere with certain experimental equipment.

A small electromagnet, producing approximately 3,000 gauss between pole pieces 2-1/2" in diameter and 2" apart, is provided to deflect these electrons vertically, so that they strike a carbon cylinder, thus producing only soft x-rays which are absorbed in a three-inch lead shield around the cylinder. This magnet can also be used for small-angle vertical steering of the proton beam.

(2) <u>Deflecting magnet.</u> An 8,000 gauss magnet is used to deflect the 32 Mev proton beam horizontally, and thus separate it from the lower components of 4 and 8 Mev. The latter are produced by protons spending 2 r.f. cycles in each drift tube space. The magnet also removes the 16 Mev H_2^+ component if a 1/4 mil

aluminum stripping foil is inserted ahead of the field. Output ports are

provided at -15°, 0°, 10°, 20° and 30°. The magnet is used primarily as a

switch, to move the beam from one experimental set up to another.

(3) Bombardment facilities. After the beam has passed through the deflecting

magnet, it is available for the bombardment of targets. Apparatus at this end

of the machine is so similar to that found in cyclotron installations, that a

description of it seems out of place in an article on a linear accelerator.

Two useful items are a Faraday cup in vacuum, for beam integration, and a rotating

foil changer, which is employed for varying the energy of the beam. Space is

available for the installation of β-ray spectrographs, cloud chambers, scattering

chambers, and other similar pieces of research equipment.

VIII. PERFORMANCE

(1) Energy. The output energy of the linear accelerator has been determined

by range measurements in aluminum, using the range energy relation as computed by

Aron, et al[18]; the energy can be varied over a range of ± 150 Kev, by moving the

"end tuners," or half drift tubes at the ends of the machine. The measured energy

on a particular day will be close to 31.7 Mev.

The energy spread of the beam can only be inferred at present from the

sharpness of the threshold of the reaction[19] $C^{12}(p,n)N^{12}$. When the resulting

excitation curve is corrected for absorber straggling, the r.m.s. energy width

of the beam can be shown to be $\Delta E < 100$ Kev on the high energy side. The

shape of the energy spectrum on the low energy side is not susceptible to

measurement by this technique. If one were to define the beam by slits, and

subject it to a magnetic deflection, the inhomogeniety introduced by the passage

of protons through the slit pairs would certainly be greater than that already

present.

In addition to the principal 32 Mev beam, there are two other beam components

(usually removed by a magnet). These are 16 Mev H_2^+ and 8 Mev H^+, particles which spend two r.f. cycles in each drift tube space and therefore emerge with half the expected final velocity.

(2) Current. For most purposes, the time average current is of most importance. During the past six months, an experimenter could be sure of having 1/4 microampere of average current, if he could use it. In many experiments, the beam is purposely cut down by a large factor. Occasionally, the beam is somewhat higher, and 0.37 μ amps is the present record value of $\overline{I}$. These values are for operation at 15 cycles per second recurrence rate. Thirty cycle operation of course doubles the current, but at the moment, the reliability of the pre-exciter is poor at this recurrence. There is no doubt that when the newly developed pre-exciter system is installed, the assumed beam will be doubled to 1/2 μ amp.

At 15 cycles per second, the pulse length is 600 μ sec, so the duty cycle is 1 in 111. The peak current at $\overline{I}$ = .375 μ amp is therefore 50 μ amp. If the grid loss is assumed to be a factor of 3 and the phase angle is assumed to be 36°, the calculated injection current agrees well with the measured injection current of 1.5 milliamps. Neither grid loss nor phase angle are well known, but these are reasonable estimates. The agreement indicates that no large gains in output current are to be had, unless major changes are made.

Several changes have been investigated, and two of them are well under way. A radio frequency "buncher" has been built and tested. Protons from the Van de Graaff are velocity modulated by the buncher, and after a drift space of 15 feet, are formed into small groups which occupy a small phase angle as they enter the accelerator. The peak output current from the accelerator has been tripled by the buncher. The energy tolerance on the injected beam must be decreased several fold to make the bunching of practical importance. (A small change in average velocity of the injected beam makes the bunch arrive

at an improper phase, so the output current is thereby decreased.) A program

to develop an energy stabilizing circuit has therefore been undertaken. The

"error signal" is generated by the proton bunches, when they pass through a

"catcher cavity" near the input end of the accelerator. One merely measures

the phase of the r.f. in the catcher cavity relative to that in the accelerator.

The energy stabilizer returns the phase difference to zero.

The second improvement is the use of electrostatic strong focusing lenses

of the Christofilos-Brookhaven[14] type. A quadrupole electrode system has been

installed in each drift tube and when it is used, the grids are removed. Under

these conditions, the external average beam has been increased to $1/2 \mu$ amp.

If the focusing voltage could be raised to its designed value, the current would

have been about 1μ amp. The increase in current with focusing voltage comes

from the larger phase angle at which the defocusing forces are counter balanced

by the electrostatic focusing forces. Unfortunately, sparking in the lenses

limited the voltage to the lower value. Deterioration of the cables has forced

us to abandon the strong focusing feature, and return to grids, but it is clear

that the difficulties would not have occurred if the machine had been designed

for strong focusing at the start. It is surprising that enough space was

available inside the drift tubes to make the test as successful as it was.

IX. ACKNOWLEDGMENTS

The design and construction of the linear accelerator was in every sense

a cooperative affair, and contributions from a large number of men are involved.

The list of authors of this article has been arbitrarily restricted to those who

had the responsibility for the major design features, and who were members of

the group for the period of two years during which the most intensive work was

done. (The first 32 Mev beam was observed less than two years after the decision

to build the machine, and another six months elapsed before reasonably steady

operation was reached. At the moment, the beam is used on the average of 12 hours

per day.) Much of the work was done by graduate students in the Department of Physics, and major contributions were made by the electrical and mechanical design groups of this laboratory.

We are indebted to Professor E. O. Lawrence for encouraging us to embark on the project. The Manhattan District of the U.S. Army Engineers gave us strong backing in the early days, and the Atomic Energy Commission continued this support. The Signal Corps generously donated large quantities of radar equipment, without which we probably would not have been able to build the accelerator.

Mr. William Baker is responsible for the redesign of the radar oscillators, without which there is a good possibility that the accelerator would never have produced a beam. Among the graduate students, special acknowledgments must be made of the valuable electronic contributions of Lawrence H. Johnston, Robert Mozley, Bruce Cork, Ernest Martinelli, Robert Phillips, Lee Aamodt, Thomas Parkin, Richard Shuey, William Toulis, Val J. Ashby, and Donald R. Cone. In the field of mechanical design, the following made important contributions: A. W. Chesterman, A. E. Kaehler, E. A. Day, R. L. Olson, D. A. Vance, Virginia McClain, Florence Mosher. The laboratory Electrical Design Group was of the greatest assistance, and we would like to acknowledge the work of Saul Lissauer, J. C. Kilpatrick, Walter Sessions, Porter Evans, and C. A. Harris.

A group of former radar technicians played an important role in the building of the machine, and some of these men are operating and servicing it at the present time. We wish to thank especially Phillip Carnahan, Albert J. Bartlett, Alva Ray Davis, Jr., Wilfred P. Kimlinger, James A. McFaden, Wendell W. Olson, and Frank Grobelch. Finally, we wish to acknowledge the important contributions in various fields, of Dr. Robert Serber, who developed the mathematical theory of beam stability, Richard Crawford, David Garbellano, Velma Turner, Leonard Deckard, and Craig Nunan. For the past few years, Robert Watt has been in charge of the operation of the accelerator. He and Craig Nunan supervised the installation of electrostatic "strong focusing" lenses, which was reported at the Brookhaven conference in December of 1952.

X.   REFERENCES

1. Sloan and Lawrence, Phys. Rev. 38, 2021 (1931).

2. Kinsey, Phys. Rev. (A), 50, 386 (1936) and private communication.

3. W. J. Sloan, Patent No. 2,398,162.

4. W. W. Hansen, Rev. Sci. Instr. 19, 89 (1948).

5. Veksler, Journ. Phys. U.S.S.R. 9, 153 (1945); McMillan, Phys. Rev. 68, 1943 (1945).

6. L. C. Slater, Rev. Mod. Phys. 20, 473 (1948).

7. H. Bradner, Rev. Sci. Instr. 19, 662 (1948).

8. R. Serber, Phys. Rev. (A), 73, 535 (1948).

9. Sperry Gyroscope Company, "Microwave Transmission Design Data."

10. F. Oppenheimer, L. H. Johnston, C. Richman, Phys. Rev. (A), 70, 447 (1946).

11. W. Panofsky, C. Richman, F. Oppenheimer, Bull. Am. Phys. Soc. 23, C8, (1948).

12. L. C. Slater, Microwave Electronics, Rev. Mod. Phys. 18, 441 (1946); Sec. 7.

13. E. M. McMillan, Phys. Rev. 80, 493 (1950).

14. J. P. Blewett, Phys. Rev. 88, 1197 (1952).

15. M. L. Good, Bull. Am. Phys. Soc. 27, No. 6 (1952).

16. L. B. Mullett, A.E.R.E. GP/M-147 (1953).

17. Baker, Edwards, Farly, and Kerns, Rev. Sci. Instr. 19, 899 (1948).

18. W. A. Aron, et al, "Range-Energy Curves," AECU-663 (1949).

19. L. W. Alvarez, Phys. Rev. 75, 1815 (1949).

+ · LINES OF H
→ LINES OF E
(E AND H ARE IN
TIME QUADRATURE)
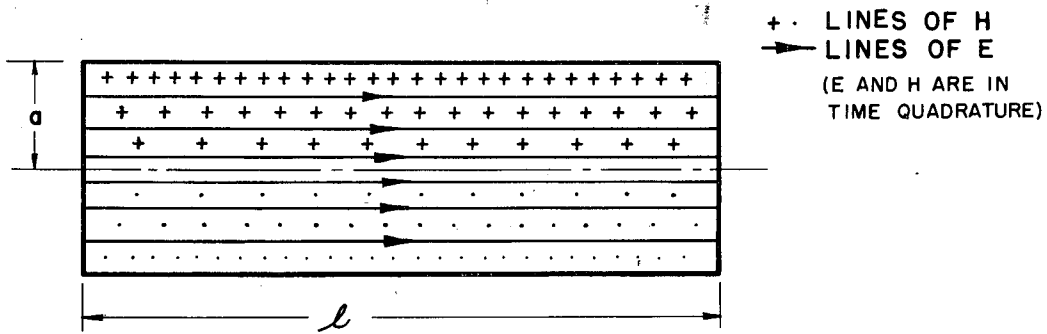
Fig. 1 Long Cylindrical Cavity Excited in Axial Electric 010 (TM_{010}) Mode.
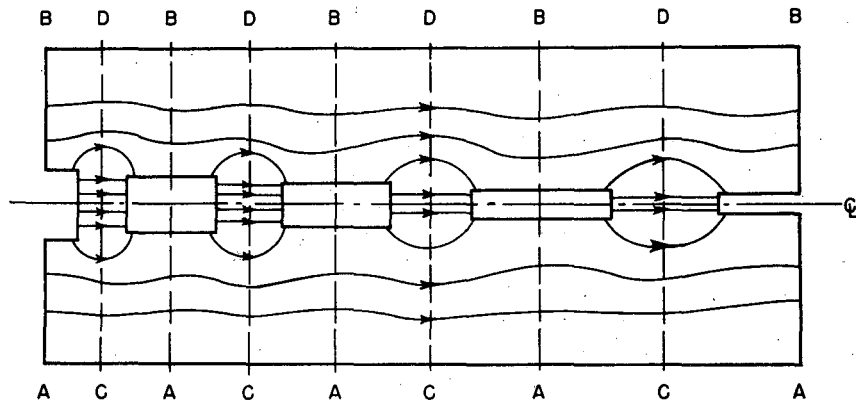
Fig. 2 Linear Accelerator Produced by Introducing Drift Tubes into
Cavity Excited as in Fig. 1. Division into Unit Cells.

$$\frac{\beta\lambda}{2}$$

R. F.
POWER
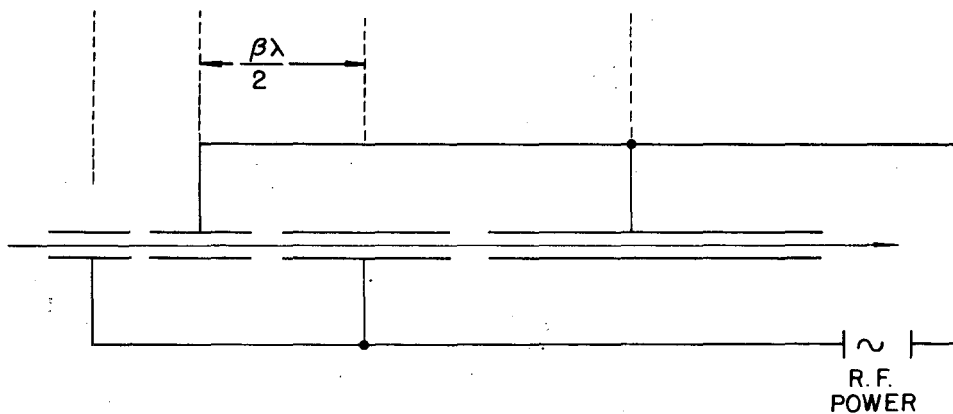
Fig. 3   Sloan-Lawrence Linear Accelerator Geometry.
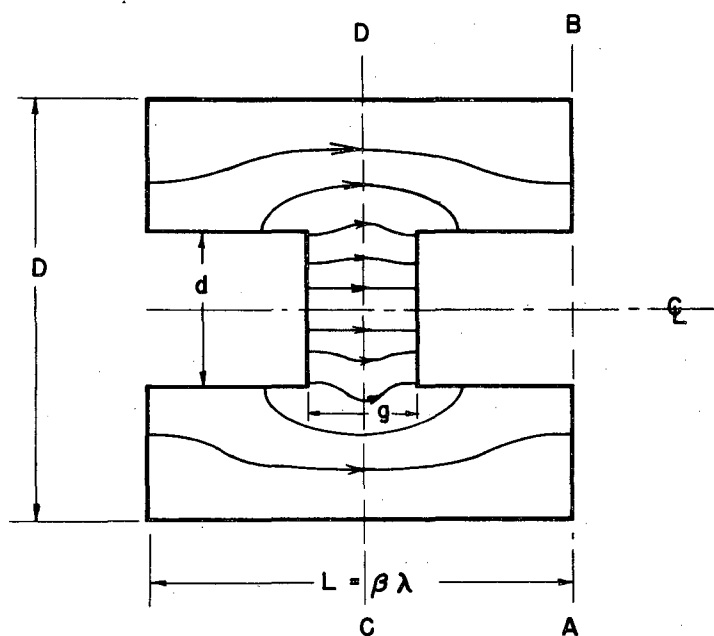
Fig. 4 Fields in "Unit Cell" of Accelerator. Note that a Conductor Across DC Would Not Change Distribution.
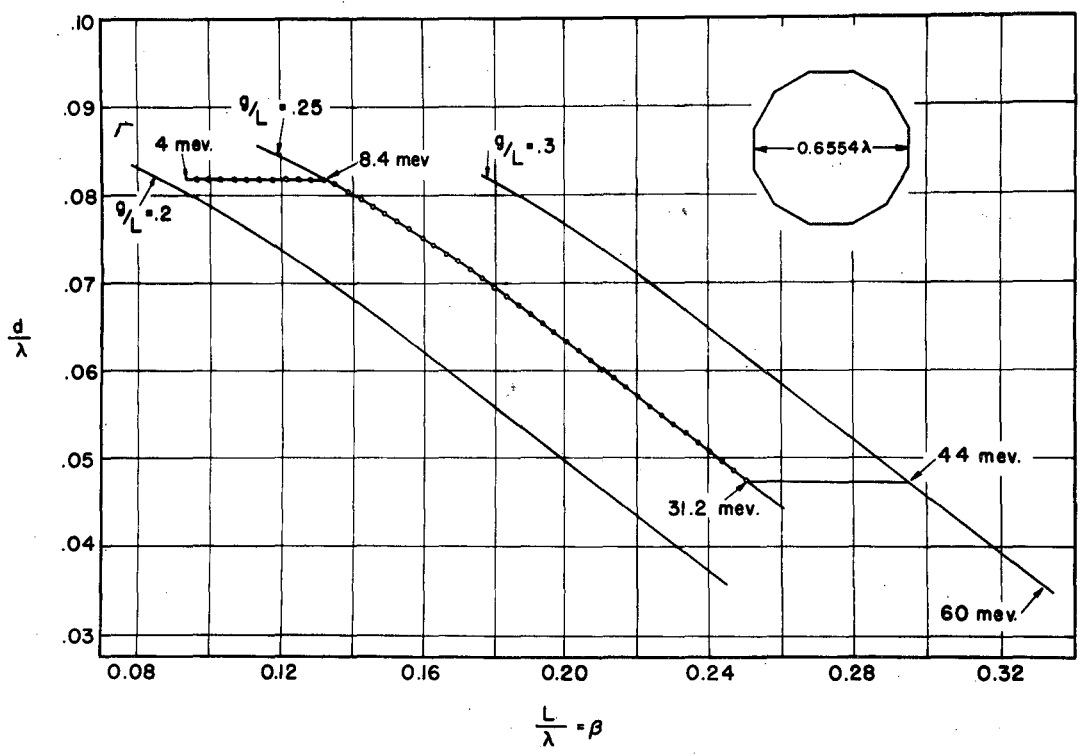
Fig. 5 Results of Model Tests on Resonant Frequencies of Re-Entrant Cavities.

EXPLORING LOOP
INTRODUCED APPROXIMATELY
⊥ TO ELECTRIC FIELD
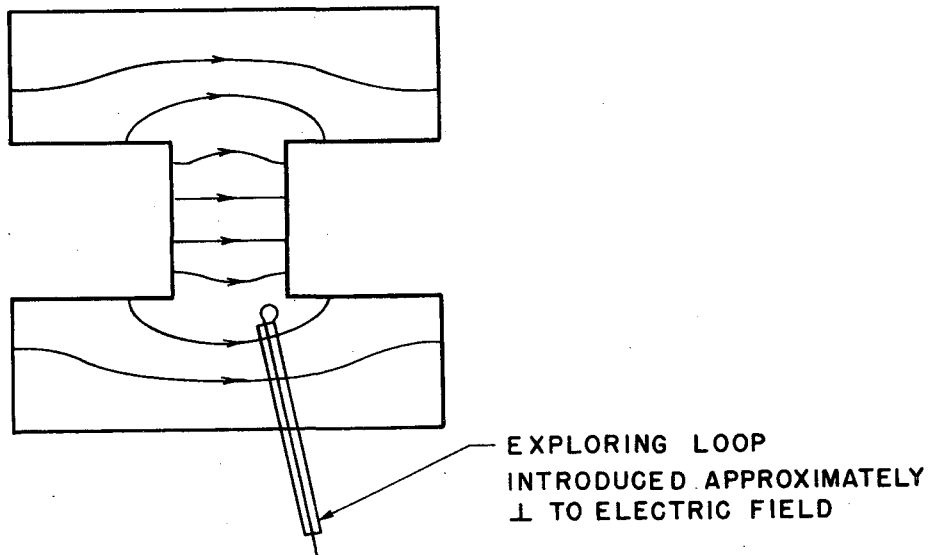
Fig. 6   Schematic Diagram Showing Magnetic Field Mapping of the Unit Cell.
         The Field Maps Permit Evaluation of the Integrals in Eq. (5) and (6).

SIMPLE THEORY - EXPERIMENT

f_n

n = 4	208.00mc.	207.16
n = 3	205.61 mc.	205.06
n = 2	203.91 mc.	203.64
n = 1	202.89 mc.	202.81
n = 0	202.55 mc.	202.55
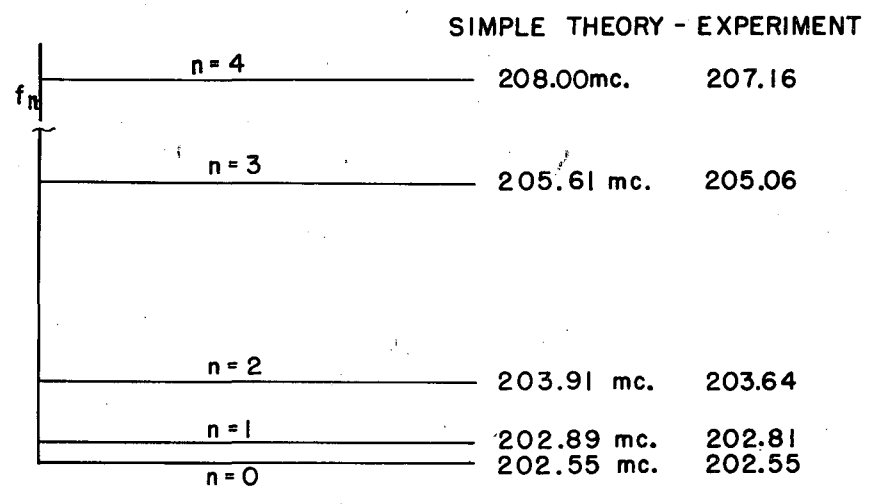
n = NUMBER OF LONGITUDINAL NODES IN THE
FIELD PATTERN.

Fig. 7   Mode Spectrum of Linear Accelerator Cavity.
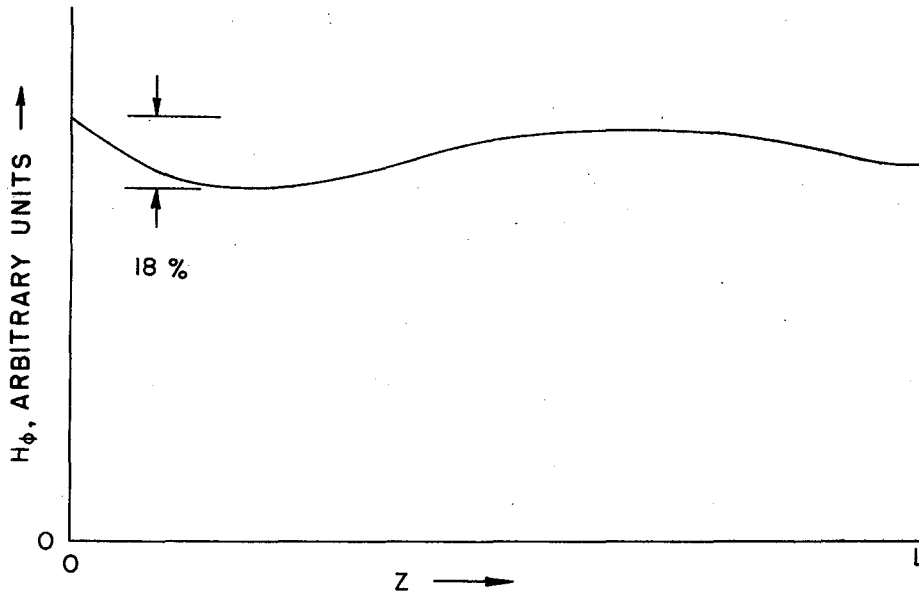
Fig. 8a   Effect of Fourier Analysis in Correcting Cavity
           [Original Hϕ (z)].

00100605628
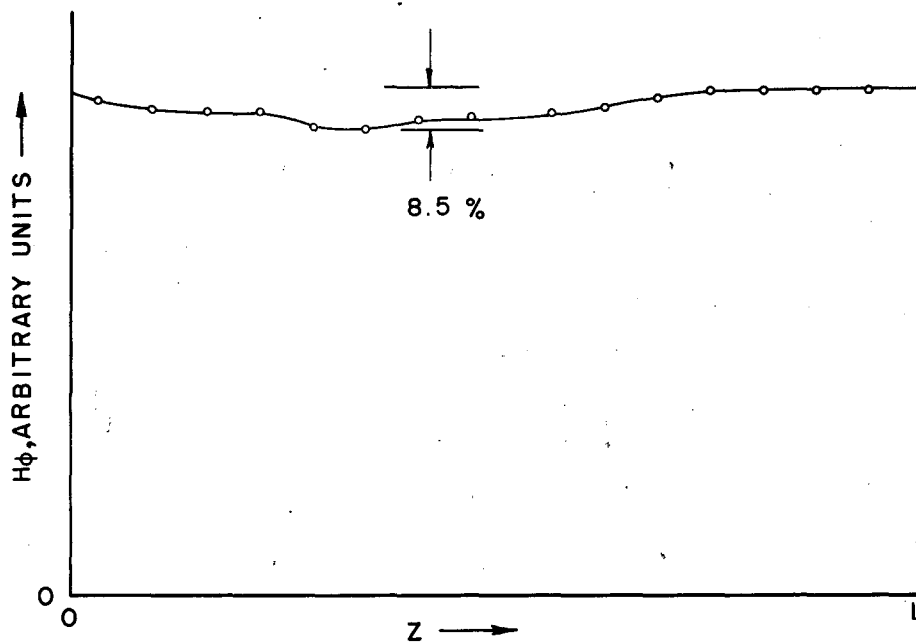
Fig. 8b Effect of Fourier Analysis in Correcting Cavity ⌊HØ (z) after Introduction of Shims ⌉.

FIGURE 8C
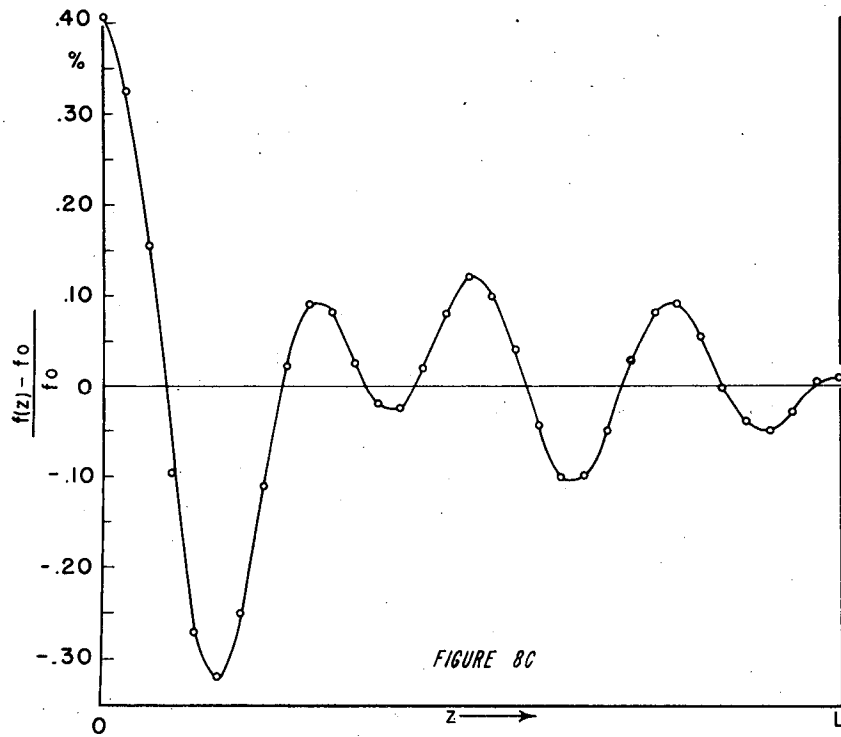
Fig. 8c   Effect of Fourier Analysis in Correcting Cavity.
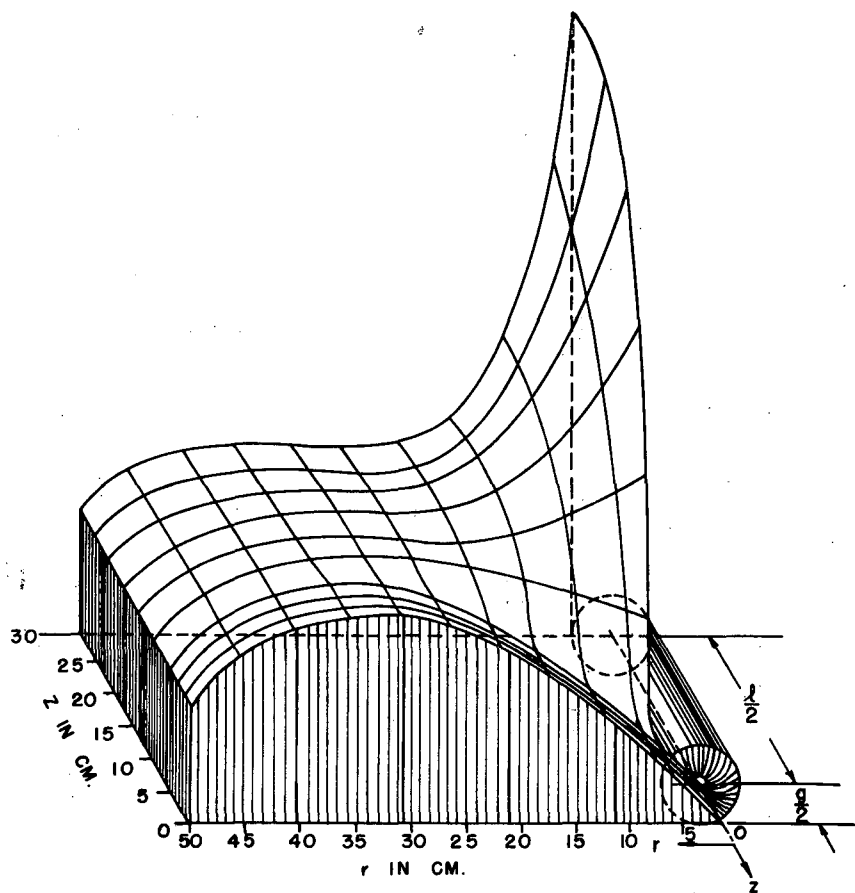
Fig. 9 Contour Plot of Magnetic Field in Typical Cavity Section.
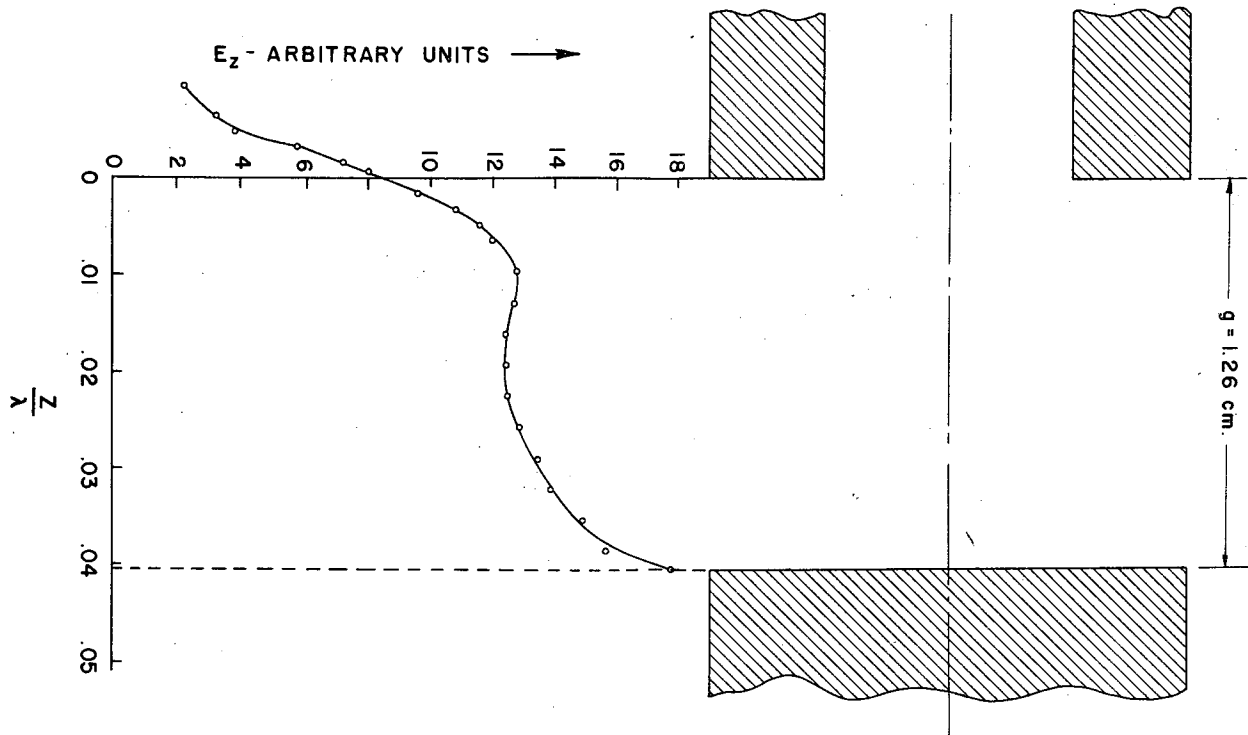
Fig. 10   Typical Axial Electric Field Plot along Drift Tube Axis.
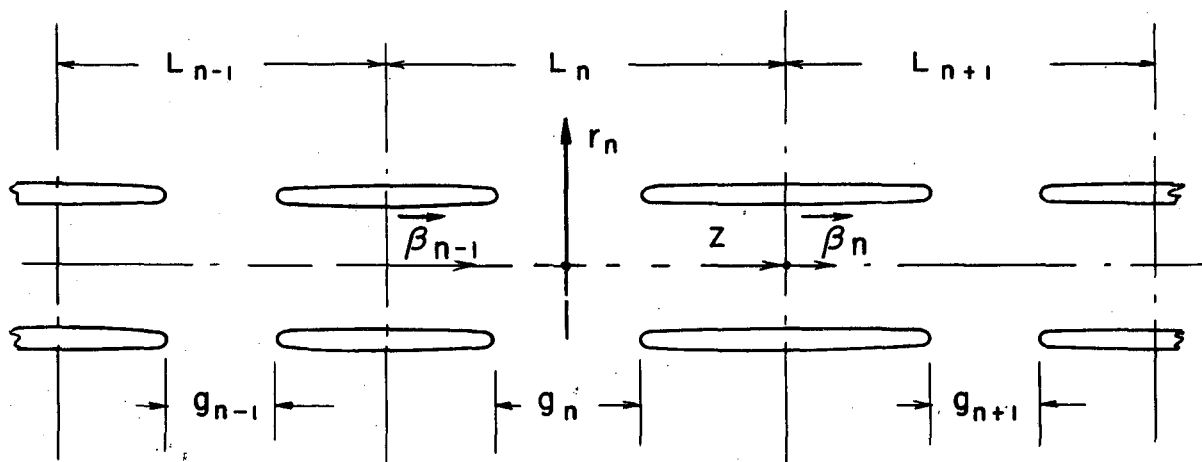
MU 1447

Fig. 11 Basic Geometry of the Linear Accelerator.
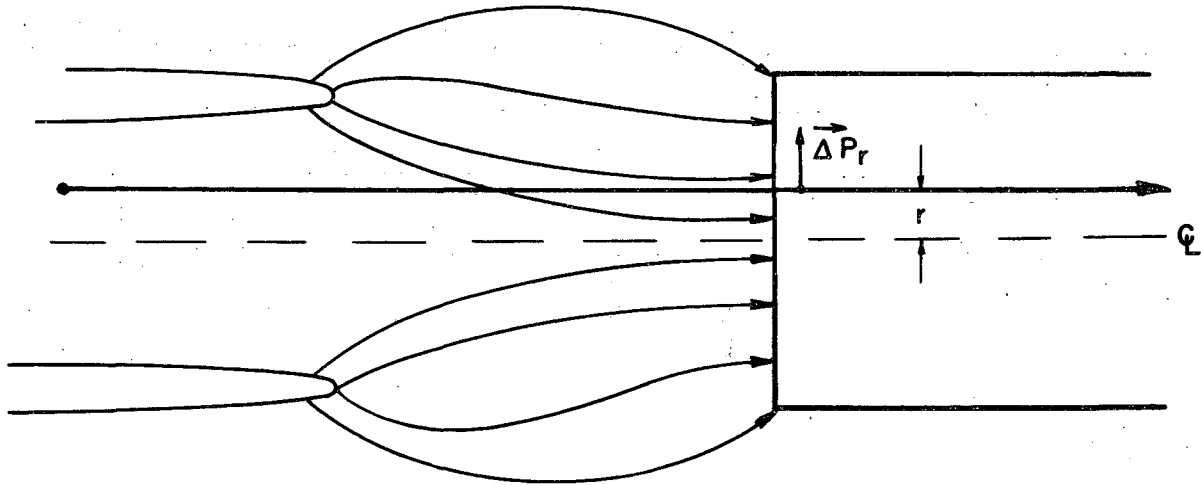
Fig. 12 Grid or Foil Geometry.

ELECTRIC FIELD AT CENTER OF GAP

Φ = PHASE OF TRANSIT ACROSS CENTER

$-\frac{\pi}{2}$ $-\frac{\pi}{4}$ 0

PHASE STABLE AND DEFOCUSING

PHASE STABLE AND FOCUSING FOR $g/L = \frac{1}{4}$
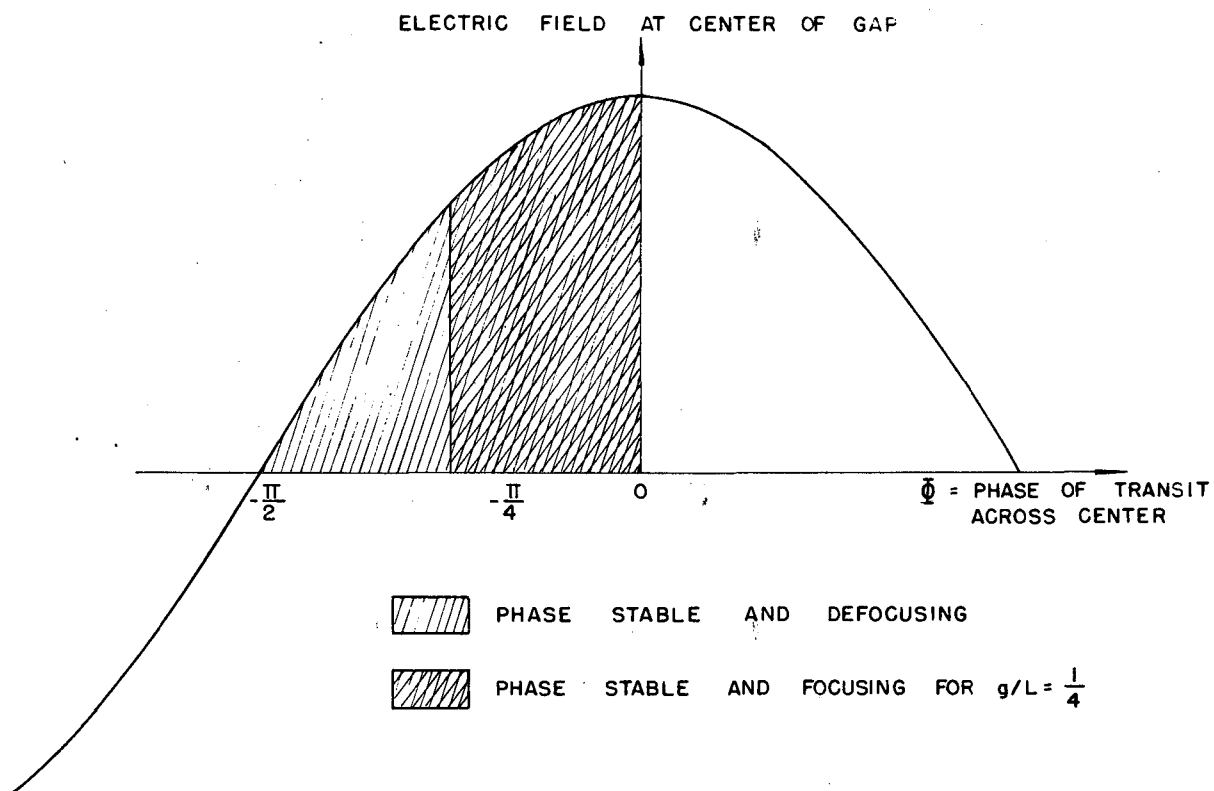
Fig. 13 Phase Diagram Indicating Definition of $\emptyset$ and Regions of
Stability in Grid Focused Operation.
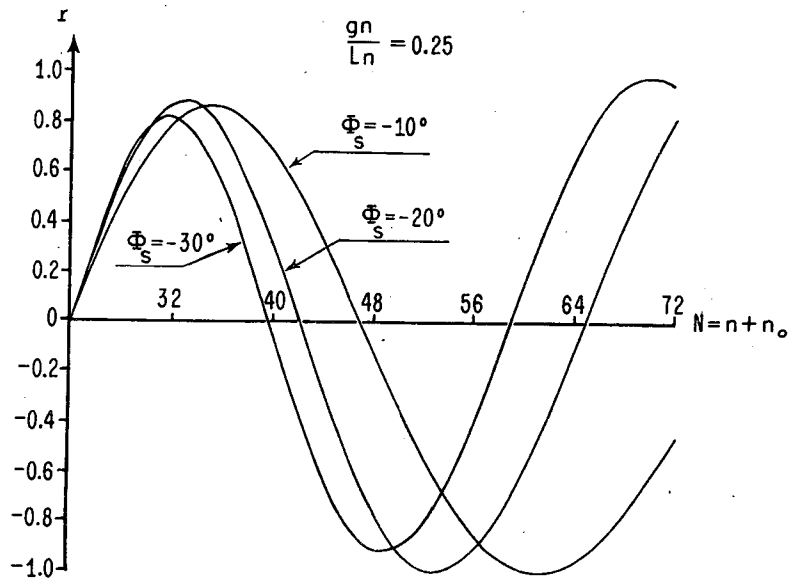
Fig. 14 Radial Oscillations of Grid or Foil Focused Linear
         Accelerator for Various Synchronous Phase Angles.
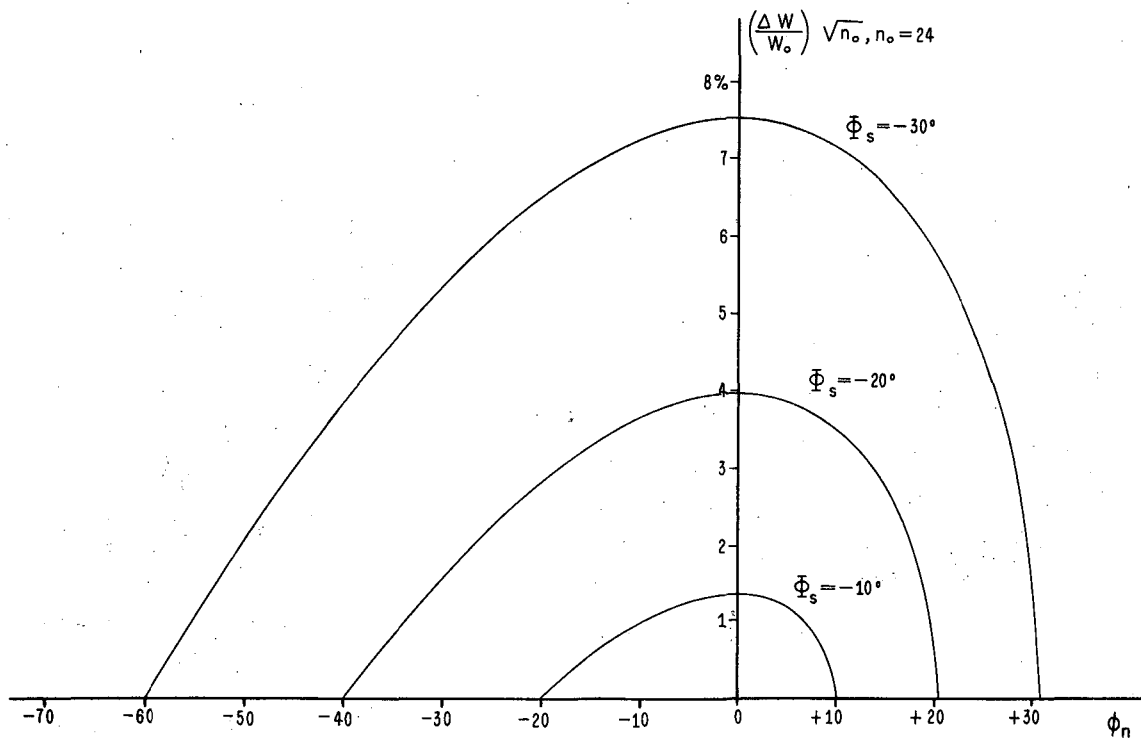
Fig. 15   Phase Acceptance of a Linear Accelerator vs. Fractional
          Variations in Injection Energy for Various Synchronous
          Phase Angles.
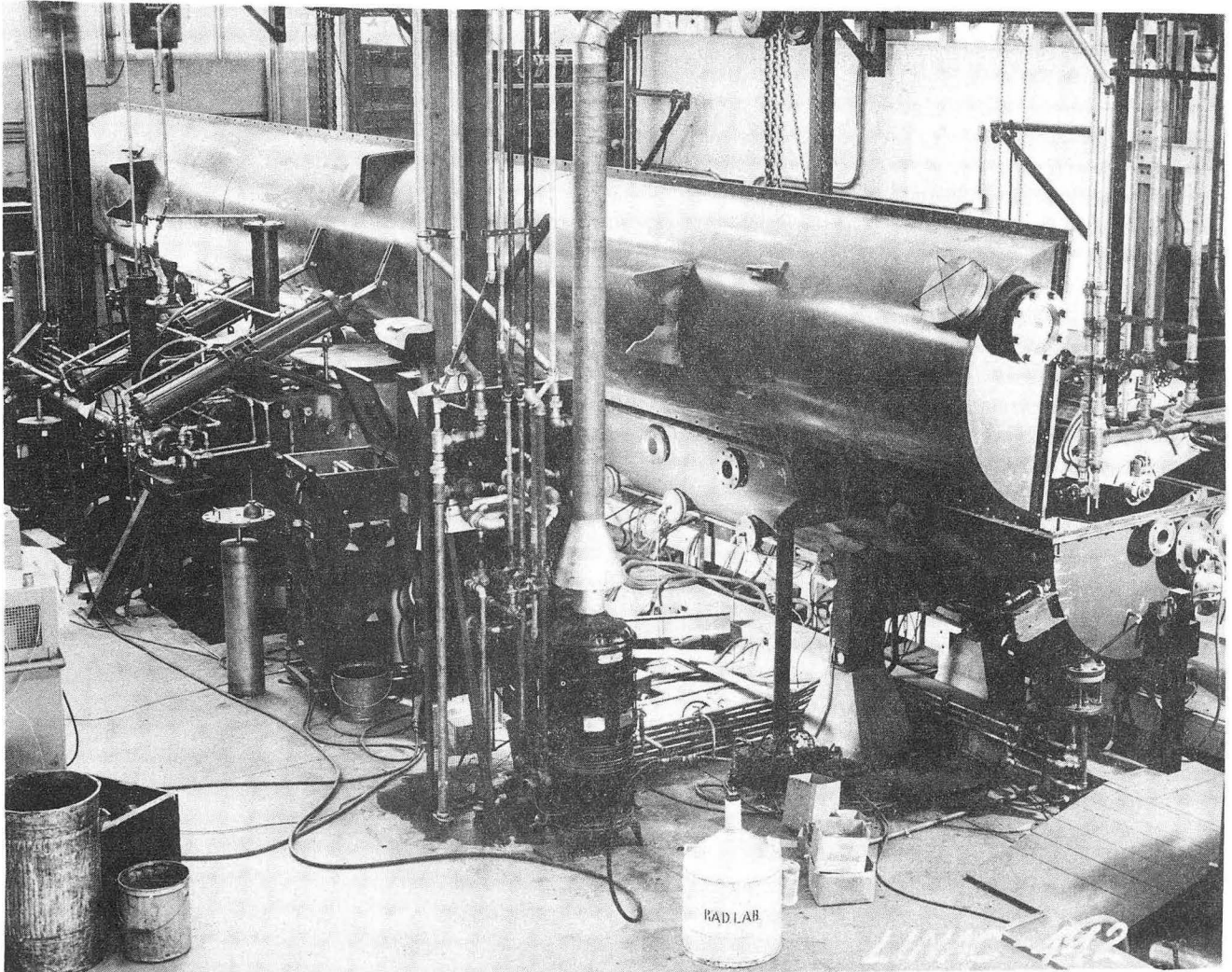
Fig. 16 Photograph of Tank Opened for Receiving Liner.
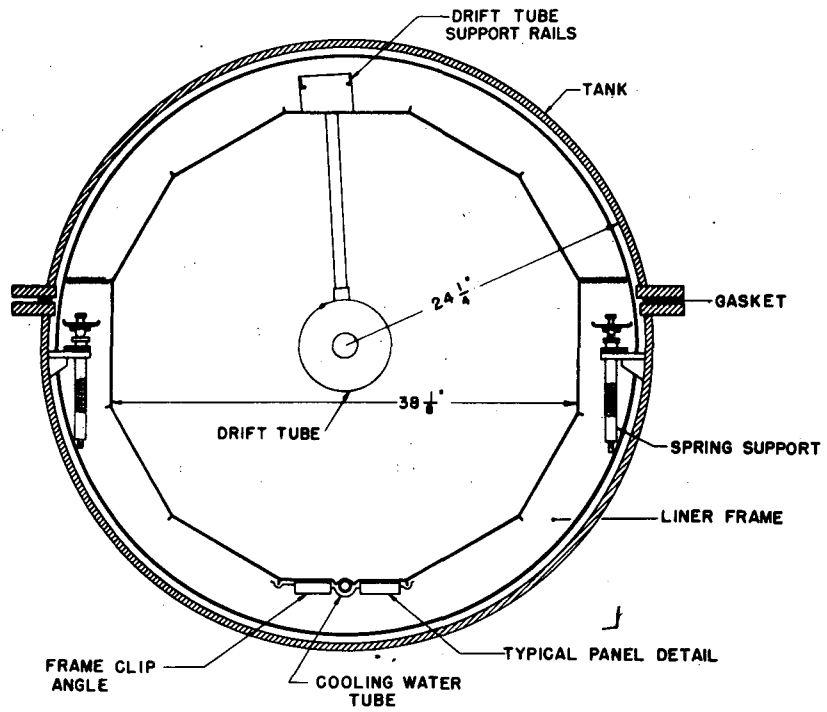
Fig. 17 Diagram Showing Disposition of Tank and Liner.
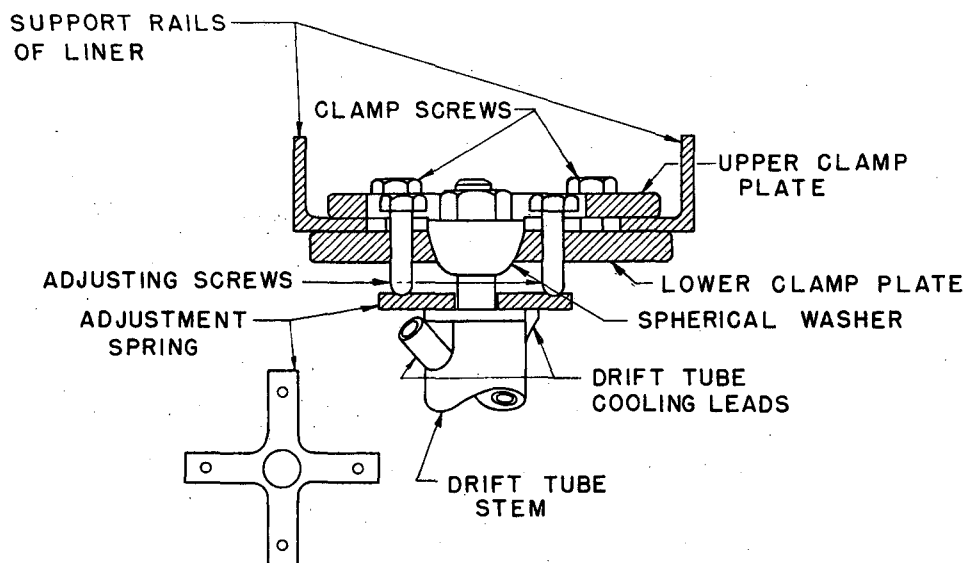
Fig. 18   Drift Tube Clamps and Arrangement.

CONTACT
FINGERS

SUPPORTING
STEM
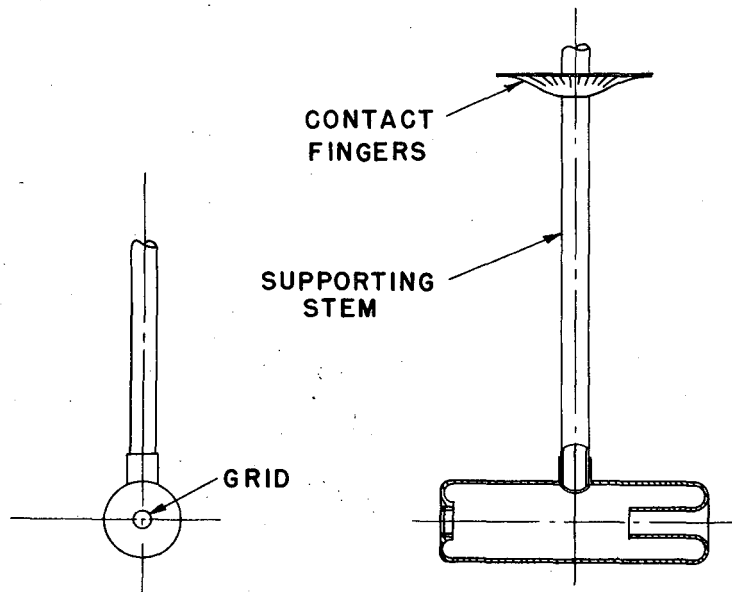
GRID

Fig. 19   Outline Drawing of Drift Tube.
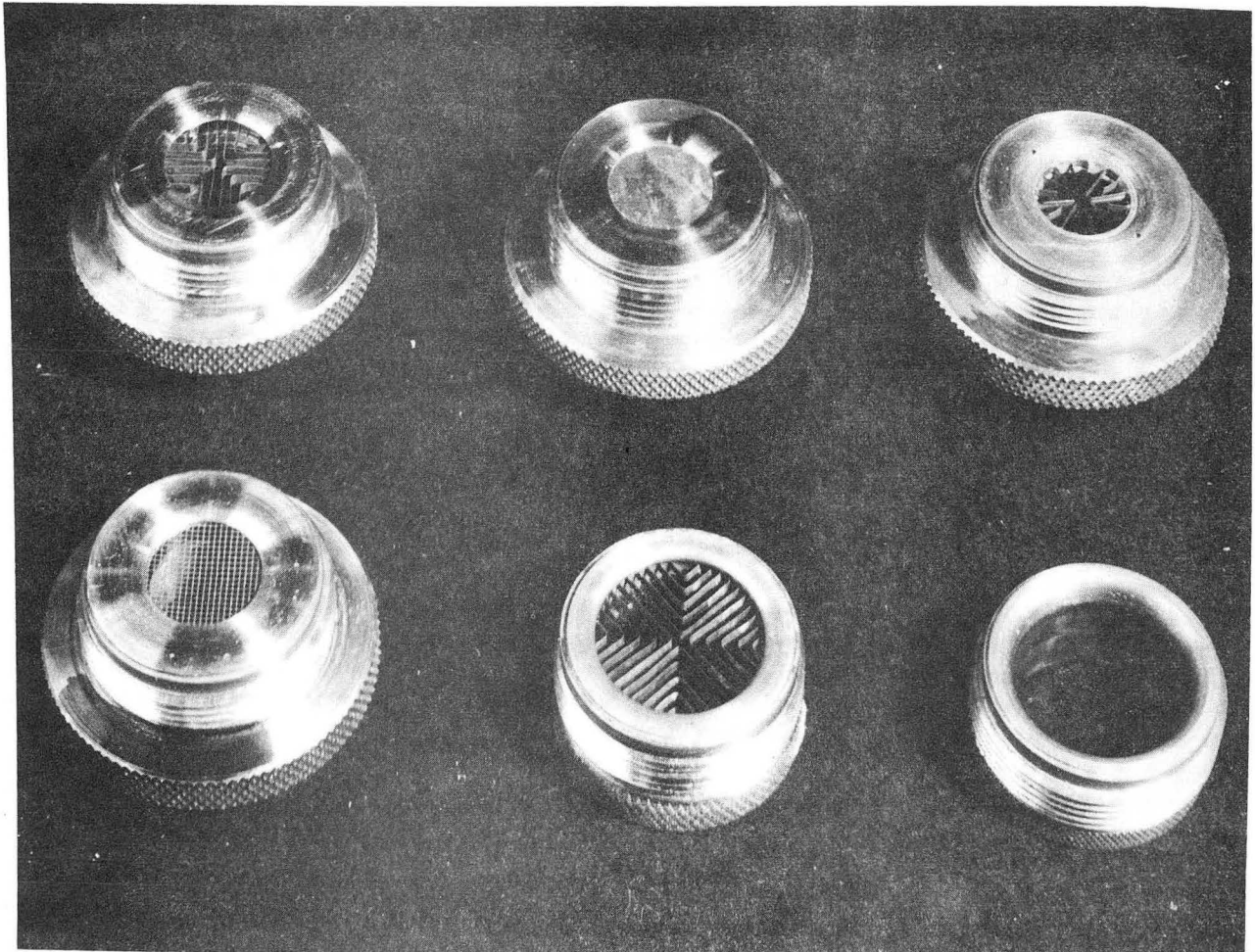
Fig. 20   Photograph of Various Types of Slat Grids and
          Beryllium Foils Mounted in Holders.
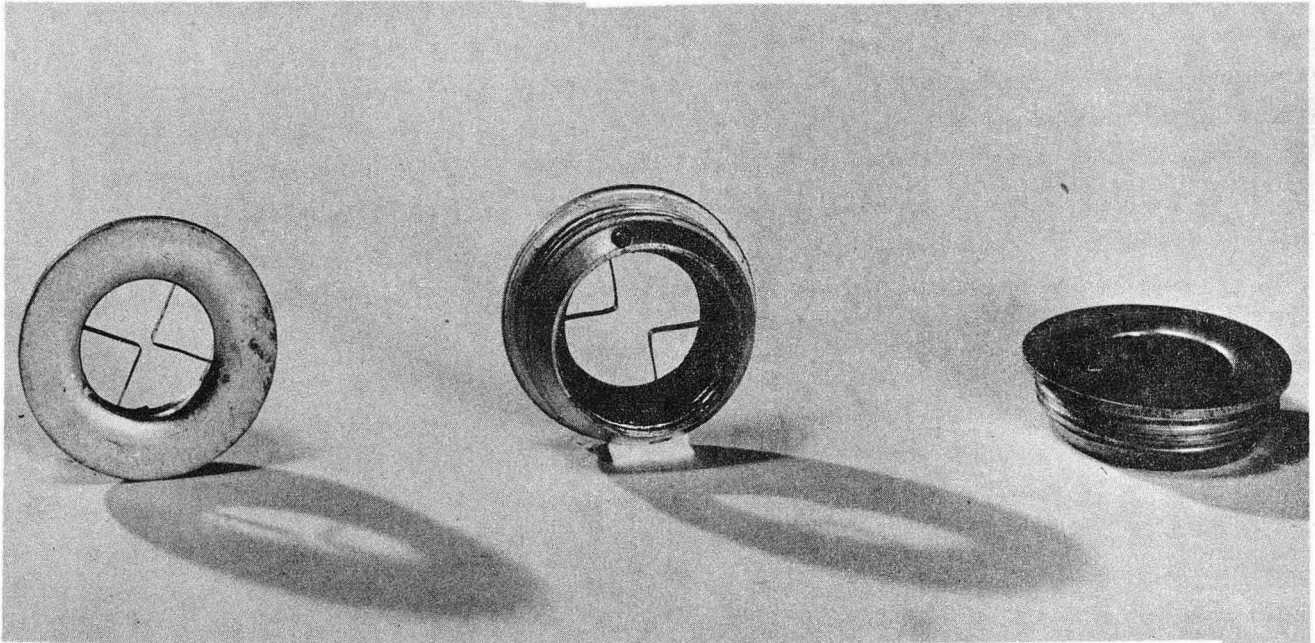
Fig. 21 Grids of the Type Now Used in the Linear Accelerator.
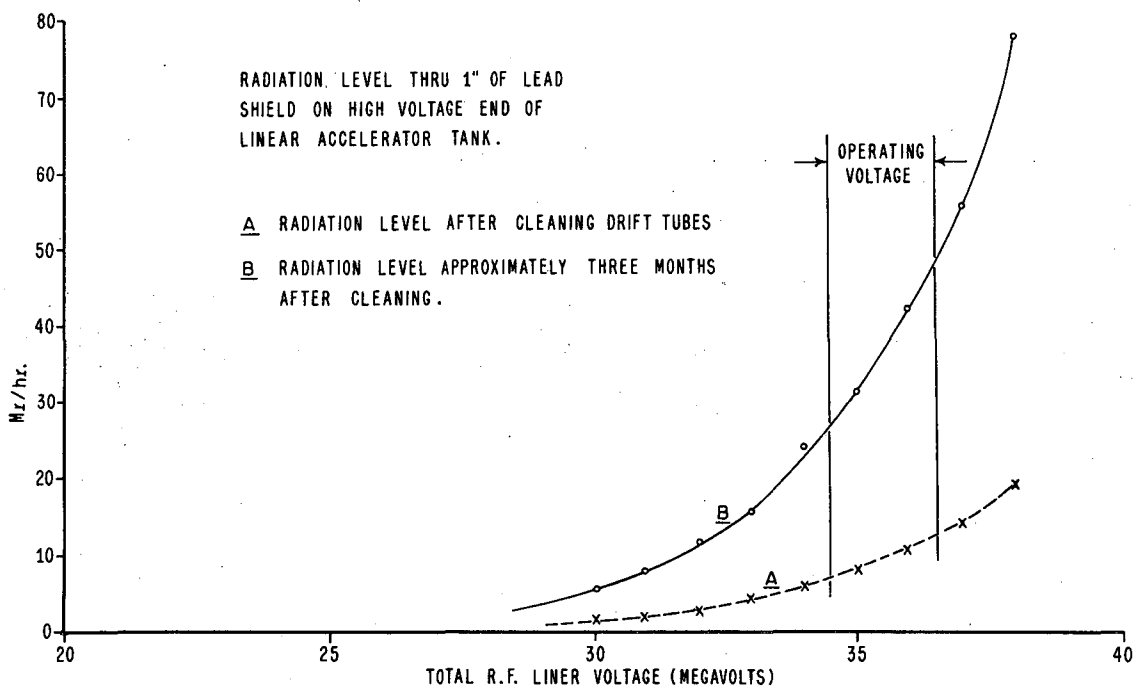
Fig. 22   X-Ray Level Near Output End of the Linear Accelerator
           as a Function of Operating Radio Frequency Voltage.
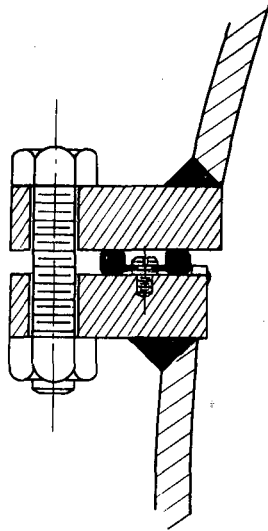
Fig. 23   Cross Section of Main Tank Gasket.
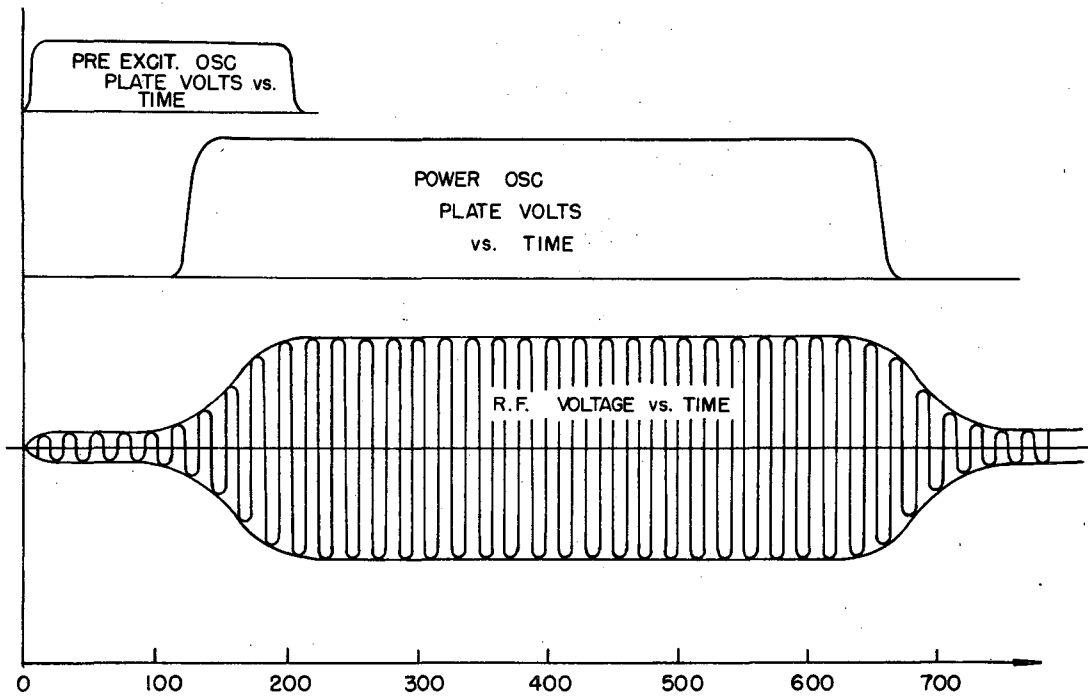
Fig. 24 Plate and R.F. Voltage vs. Time.

AIRFLOW INTERLOCK SWITCH

OSCILLATOR HOUSING

COOLING AIR (CATHODE)

R.F. TRANSMISSION LINE

OSCILLATOR COUPLING LOOP

R.F. INSULATOR

VACUUM SEALS

TRANSMISSION LINE OUTER VACUUM SEAL

R.F. LINER

FLANGE FOR MECHANICAL MOUNTING OF OSC.

VACUUM TANK

LUCITE INSULATOR, AIR BAFFLE AND MECHANICAL SUPPORT

GRID CONNECTOR

TRIODE VACUUM TUBE (3W10000A3)

COOLING AIR (GRID SEAL)

FILAMENT AND CATHODE CONNECTORS

PLATE D.C. BLOCKING CAPACITOR

Fig. 25 Cross Sectional View of Oscillator and Transmission Line.

TRANSMISSION LINE STUB $\frac{\lambda}{4}$ USED
AS MECHANICAL SUPPORT AND TO
BRING IN COOLING AIR AND CATHODE
POWER TO OSC. TUBE

$\frac{\lambda}{2}$ (APPROX.)

$\frac{\lambda}{4}$ (APPROX.)

COUPLING LOOP

OUTPUT TRANSMISSION LINE

DRIVE CIRCUIT (GRID TO CATHODE)

OUTPUT CIRCUIT (GRID TO PLATE)

$\frac{\lambda}{2}$ (APPROX.)

$\frac{\lambda}{2}$ (APPROX.)

PLATE H.V.

D.C. PLATE BLOCKING CONDENSER

$\underline{Z}_d$ (IMPEDANCE OF DRIVE CIRCUIT)

$\underline{Z}_L$ (IMPEDANCE OF LOAD CIRCUIT)

R_L C_L

CATHODE R_d $-R_T$

C_d L

GRID   PLATE Z_r (IMPEDANCE OF TUBE AS GENERATOR)

DETAIL A

EQUIVALENT LUMPED CONSTANT IMPEDANCES
AT JUNCTION OF TRANSMISSION LINES.

C_L R_L

L

C_d R_d

EQUIVALENT CIRCUIT

Fig. 26   Linac Oscillator Schematic.
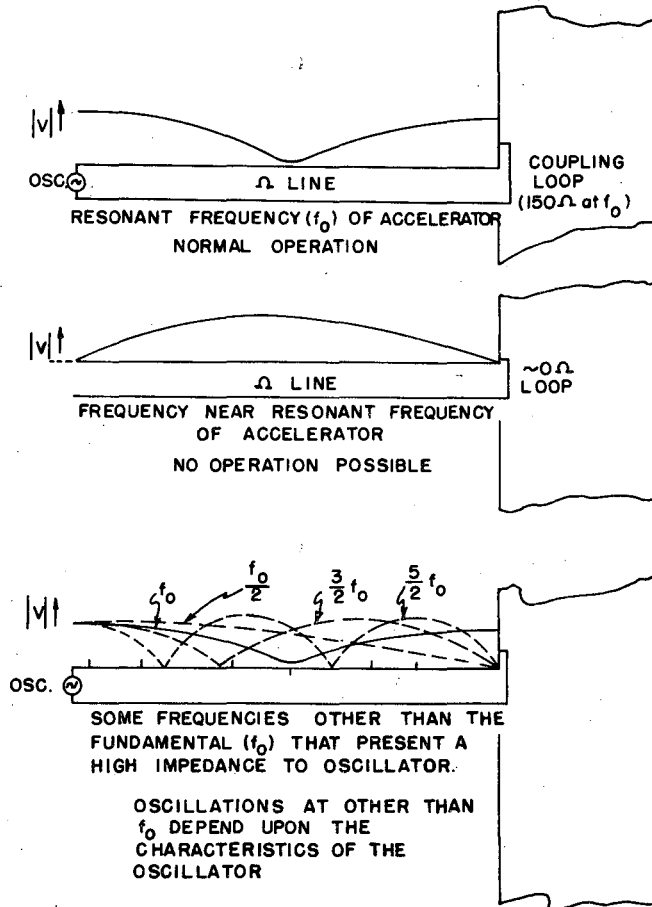
Fig. 27   Voltage Distribution along Transmission Line for Correct
          and Incorrect Modes of Operation.
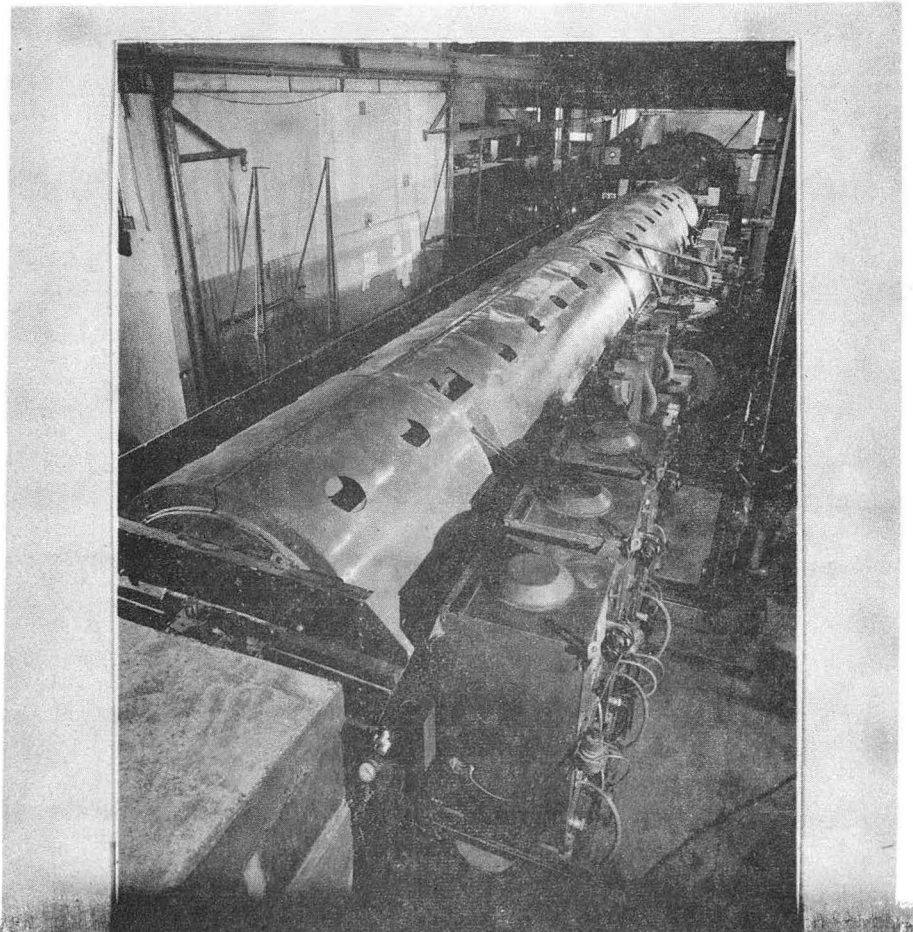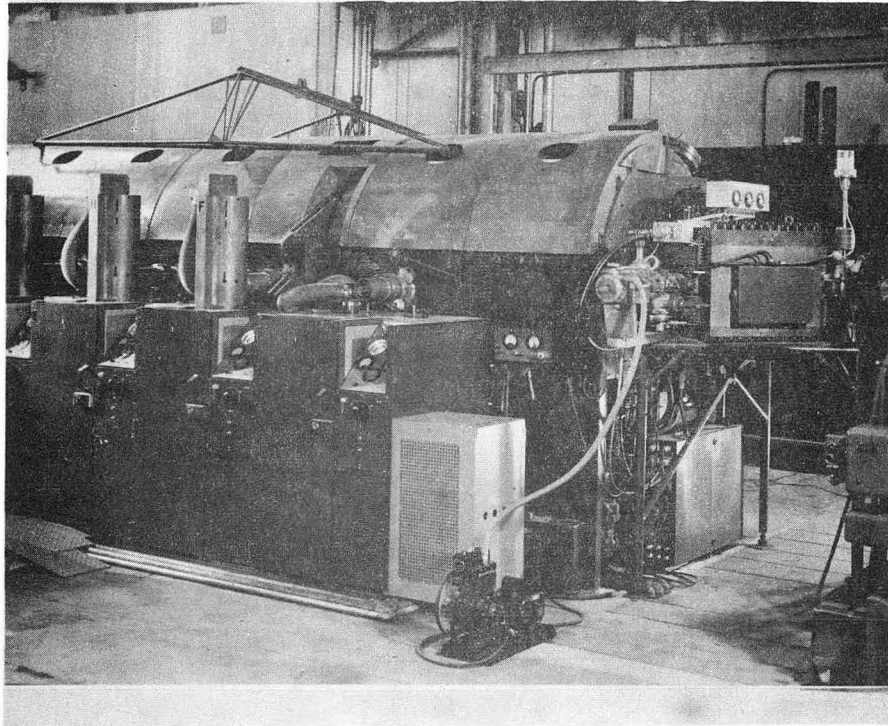
Fig. 28a and 28b Oscillators Installed on the Linear Accelerator
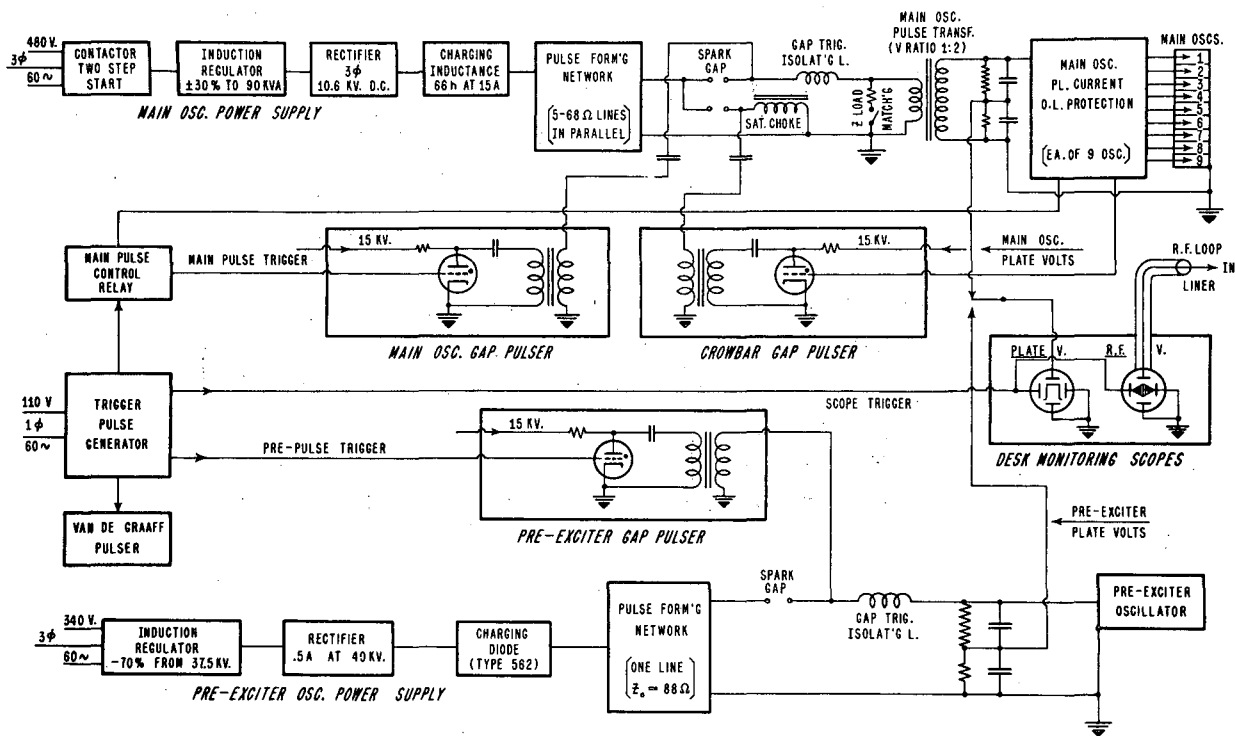
Fig. 29 Block Diagram Power Supply System.

Fig. 30 Schematic Diagram of Pulse-forming Line.
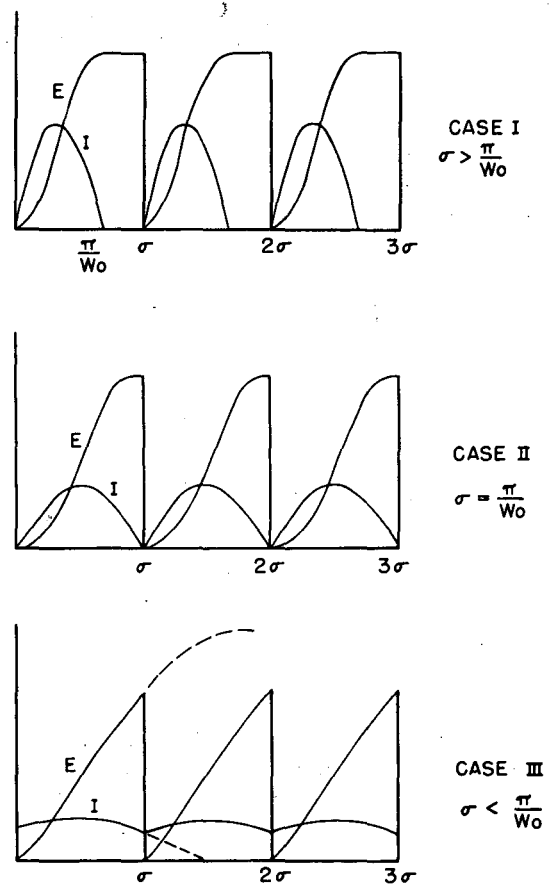
Fig. 31 Pulse Shapes Obtained in Charging of Pulse – Forming Line.